Knockdown of Ketohexokinase Versus Inhibition of Its Kinase Activity Exert Divergent Effects on Fructose Metabolism

Se-Hyung Park[1], Taghreed Fadhul[1], Lindsey R. Conroy[2], Harrison Clarke[2,3], Ramon C. Sun[2,3], Kristina Wallenius[4], Jeremie Boucher[4,5,#], Gavin O'Mahony[6], Alessandro Boianelli[7], Marie Persson[7], Sunhee Jung[8], Cholsoon Jang[8], Analia S. Loria[9], Genesee J. Martinez[9], Zachary A. Kipp[9], Evelyn A. Bates[9],Terry D. Hinds, Jr.[9], Senad Divanovic[10], and Samir Softic[1,9,11]

[1] Department of Pediatrics and Gastroenterology, University of Kentucky, Lexington, KY, USA
[2] Department of Molecular and Cellular Biochemistry, University of Kentucky, Lexington, KY, USA
[3] Department of Biochemistry & Molecular Biology, Center for Advanced Spatial Biomolecule Research, University of Florida, Gainesville, FL, USA
[4] Bioscience, Research and Early Development, Cardiovascular, Renal and Metabolism (CVRM), BioPharmaceuticals R&D, AstraZeneca, Gothenburg, Sweden.
[5] The Lundberg Laboratory for Diabetes Research, Department of Molecular and Clinical Medicine, Sahlgrenska Academy, University of Gothenburg, Gothenburg, Sweden
[6] Medicinal Chemistry, Research and Early Development, Cardiovascular, Renal and Metabolism (CVRM), BioPharmaceuticals R&D, AstraZeneca, Gothenburg, Sweden.
[7] DMPK, Research and Early Development, Cardiovascular, Renal and Metabolism (CVRM), BioPharmaceuticals R&D, AstraZeneca, Gothenburg, Sweden
[8] Department of Biological Chemistry, School of Medicine; Center for Epigenetics and Metabolism; Chao Family Comprehensive Cancer Center, University of California Irvine, Irvine, CA 92697
[9] Department of Pharmacology and Nutritional Sciences, University of Kentucky, Lexington, KY, USA
[10] Department of Pediatrics, University of Cincinnati College of Medicine, Division of Immunobiology, Cincinnati Children's Hospital Medical Center, Cincinnati, OH 45229.
[11]Joslin Diabetes Center and Department of Medicine, Harvard Medical School, Boston, MA, USA
[#] Current address Metabolic Disease, Evotec International GmbH, Göttingen, Germany.

Corresponding author:

Samir Softic, MD
Associate Professor of Pediatrics, University of Kentucky
900 South Limestone, Wethington Rm 527, Lexington, KY 40536
Phone: (859) 218-1379
Fax: (859) 257-7799
E-mail: samir.softic@uky.edu

CONFLICT OF INTEREST

SS received grant funding from Alnylam Pharmaceuticals, Inc., to study the KHK biology. Alnylam also provided KHK siRNA and performed F1P quantification. This work was also supported by AstraZeneca who provided the KHK inhibitor, 3-OMF, and performed pharmacokinetic studies. K.W., J.B., G.O., A.B., and M.P. are/were employees of AstraZeneca.

ABSTRACT

Excessive fructose intake is a risk factor for the development of obesity and its complications. Targeting ketohexokinase (KHK), the first enzyme of fructose metabolism, has been investigated for the management of MASLD. We compared the effects of systemic, small molecule inhibitor of KHK enzymatic activity to hepatocyte-specific, GalNAc-siRNA mediated knockdown of KHK in mice on a HFD. We measured KHK enzymatic activity, extensively quantified glycogen accumulation, performed RNAseq analysis, and enumerated hepatic metabolites using mass spectrometry. Both KHK siRNA and KHK inhibitor led to an improvement in liver steatosis, however, via substantially different mechanisms. KHK knockdown decreased the de novo lipogenesis pathway, whereas the inhibitor increased the fatty acid oxidation pathway. Moreover, KHK knockdown completely prevented hepatic fructolysis and improved glucose tolerance. Conversely, the KHK inhibitor only partially reduced fructolysis, but it also targeted triokinase, mediating the third step of fructolysis. This leads to the accumulation of fructose-1 phosphate, resulting in glycogen accumulation, hepatomegaly, and impaired glucose tolerance. Overexpression of wild-type, but not kinase-dead KHK in cultured hepatocytes increased hepatocyte injury and glycogen accumulation when treated with fructose. The differences between KHK inhibition and knockdown are, in part, explained by the kinase-dependent and independent effects of KHK on hepatic metabolism.

INTRODUCTION

High intake of dietary sugar has undoubtedly been linked to the development of obesity-associated complications, such as metabolic dysfunction associated steatotic liver disease (MASLD). Therefore, the World Health Organization (1), and several leading medical societies, such as the American Heart Association (2), Canadian Diabetes Association (3), and three European medical groups (EASL, EASD, EASO) (4) recommend reducing sugar intake as a way to ameliorate metabolic dysfunction.

The adverse effects of sugar have mainly been attributed to its fructose component. Several properties of dietary fructose make it uniquely suitable to promote the development of obesity-associated complications, such as MASLD (5). Fructose strongly enhances hepatic de novo lipogenesis (DNL) by acting as both a substrate for fatty acid synthesis and by upregulating SREBP1c and ChREBP lipogenic transcription factors (6, 7). On the other hand, fructose restriction improves hepatic steatosis (8), and lowers body mass index (9). Furthermore, fructose decreases fatty acid oxidation (FAO) (10), either indirectly through DNL intermediate malonyl-CoA or directly through suppression of carnitine palmitoyltransferase 1a (CPT1α) (11). Additionally, fructose has been proposed to induce hepatic insulin resistance (12), elevate uric acid production (13), promote endoplasmic reticulum stress (14), and propagate mitochondrial dysfunction (15). Indeed, fructose consumption is 2-3 fold higher in adults with biopsy-confirmed MASLD (16), and correlates with a higher incidence of liver fibrosis (17).

The effects of dietary fructose are dependent on its catabolism via ketohexokinase (KHK), the first enzyme of fructolysis. Thus, mice with whole-body knockout of KHK on an obesogenic diet are protected from MASLD (18, 19). We and others have shown that liver-specific deletion of KHK is sufficient to reverse MASLD (7, 20). Based on the strong premise that fructose contributes to metabolic dysfunction and that KHK deletion prevents it, has led to the development of small molecule inhibitors of KHK enzymatic activity. The inhibitors target the ATP binding domain of KHK, which prevents fructose phosphorylation to fructose-1 phosphate (F1P) (21). Phosphorylation of fructose, similar to the phosphorylation of glucose, is required for its downstream metabolism. An early KHK inhibitor was efficacious in preclinical studies (22), but this compound has not been tested in clinical trials. Many

enzymes contain an ATP binding domain, so the initial inhibitors were not selective enough for KHK activity. Within the last decade, a new class of compounds, allegedly 600 times more specific for KHK activity, have been developed. These inhibitors were likewise found to effectively reduce steatosis in rats (23), but also in human liver tissue (24). Moreover, recent clinical trials reported that the new KHK inhibitors significantly reduced whole liver fat in patients with MASLD (25, 26). Despite the positive data, the leading developer unexpectedly announced that they are stopping further advancement of the KHK inhibitor (27).

In this study, we compared head-to-head the effects of systemic, small molecule KHK inhibitor (PF-06835919) versus liver-specific knockdown (KD) of KHK using GalNAc-conjugated siRNA. Our laboratory was the first to suggest that KHK has kinase-independent functions (28, 29). We hypothesize that inhibiting only the kinase function of KHK may not be sufficient to fully reverse metabolic dysfunction associated with fructose intake. This hypothesis may explain why KHK inhibitors have not progressed in clinical development despite preclinical studies consistently showing the benefits of KHK knockout.

RESULTS

Inhibition of ketohexokinase activity, but not its knockdown, leads to hepatic glycogen accumulation.

To compare the effects of liver-specific KHK knockdown using siRNA versus systemic small-molecule inhibitor of KHK kinase activity, we placed male, C57Bl6/J, mice on a LFD or a HFD for six weeks. Thereafter, the mice on a high-fat diet were subdivided into three groups; the control group (HFD), the KHK siRNA group (HFD+siRNA) and the KHK inhibitor group (HFD+Inhib). All mice were injected with luciferase control siRNA (10 mg/kg), or siRNA targeting total KHK (20mg/kg) every two weeks. Additionally, all mice were gavaged methylcellulose control or (15mg/kg) KHK inhibitor (PF-06835919) in methylcellulose, twice daily for four weeks (Figure S1A). The inhibitor dose was set to achieve exposure in mice that had previously been shown to achieve over 90% KHK inhibition in rats (23). The mice were treated with the drugs for four weeks. The mice in the HFD group weighed significantly more than the mice on a LFD (37.8±1.1g vs. 27.5±0.9g) (Figure 1A, S1B). KD of KHK (36.3±0.9g) or inhibition of its kinase activity (35.5±0.8g) did not significantly reduce body weight. Caloric intake was increased in all mice on a HFD, but there was no difference among the groups (Figure S1C). Similarly, water intake was not different among the HFD groups (Figure S1D). Body composition assessed by echoMRI revealed a lower percent lean mass in the HFD (66.8±3.3%), compared to the LFD group (85.4±1.2%) (Figure 1B). KD of KHK induced no change (65.1±1.4%), while inhibition of KHK increased the percent lean mass (72.9±1.8%). Conversely, the percent body fat was higher in mice on a HFD (30.5%±3.2) compared to the LFD group (11.3±1.3%). The HFD+siRNA group (32.6±1.4%) was not different, while the percent fat decreased in the HFD+Inhib group (24.2±2.0%). This could be accounted by lower perigonadal adipose tissue weight in the HFD+Inhib group (Figure 1C), while increased lean mass likely reflects higher liver weight in these mice (Figure 1D). Besides the liver, the kidneys and intestines effectively metabolize fructose via KHK (30). Kidney weight was not altered (Figure S1E) and intestinal histology was unchanged among the groups (Figure S1F).

A surprising increase in liver weight in the HFD+Inhib group could not be explained by steatosis (Figure S1G), as Oil Red-O staining of lipids (Figure S1H) and liver triglycerides (Figure S1I) decreased

in both the HFD+siRNA and HFD+Inhib groups, compared to the HFD. In agreement with liver steatosis, serum triglycerides decreased in both the KHK siRNA and inhibitor groups (Figure S2A), while serum cholesterol, which in mice mainly consists of HDL cholesterol, was increased only in the inhibitor-treated mice (Figure S2B). The increased liver weight agreed with the periodic acid-Schiff (PAS) staining, suggesting that glycogen was higher in the HFD+Inhib group (Figure 1E). Indeed, mass spectrometry quantification revealed elevated glycogen levels only in the HFD+Inhib group, compared to the LFD group (Figure 1F). Glycogen accumulation is partially controlled by glucagon. We found reduced glucagon concentration in the HFD+Inhib group (39±4pg/ml), compared to both HFD (63±7pg/ml) and HFD+siRNA groups (62±6 pg/ml) (Figure S2C). Next, we quantified the glycogen chain length and found that only the HFD+Inhib group had an increased abundance of glycogen composed of short glucose polymers (Figure 1G). N-linked glycans are homo- or heteropolymers of monosaccharides attached to a protein. A heatmap showed glycans were higher in the HFD compared to the LFD group (Figure 1H). Glycans decreased in the HFD+siRNA group but were the highest in the HFD+Inhib group, indicative of greater monosaccharide availability. Principal component analysis of all glycans confirmed differential clustering in the HFD versus LFD groups and with KHK inhibition versus knockdown (Figure 1I). Together, these data indicate that mice in the HFD+Inhib group had increased glycogen accumulation and greater monosaccharide availability.

To interrogate the mechanism behind increased glycogen accumulation, we quantified the expression of glucokinase (Gck), which was increased two-fold in all mice on HFD but was not altered by KHK KD or inhibition (Figure 1J). In its inactive state, GCK is sequestered in the nucleus by glucokinase regulatory protein (GCKRP). The HFD and HFD+siRNA groups had 1.3 to 1.4-fold higher Gckrp expression than the LFD group (Figure 1K). The HFD+Inhib group did not have elevated Gckrp mRNA, suggesting that GCK was more active. Indeed, GCK activity was elevated in the HFD+Inhib group (Figure S2D). GCK activity stimulates glycogen synthase (Gys2), which was 1.5 to 1.7-fold higher in the HFD and HFD+siRNA groups and 2.4-fold higher in the HFD+inhib group (Figure 1K). Conversely, glycogen phosphorylase (Pygl), which liberates glucose from glycogen, was only elevated in mice on a HFD. In summary, both knockdown and inhibition of KHK improved hepatic steatosis, but KHK inhibition

increased liver weight, in part due to higher glycogen accumulation.

Similar effects were also observed in mice fed a high-fat, high-sugar diet. The mice consumed 60% HFD supplemented with 30% fructose in drinking water for ten weeks and were treated with KHK siRNA or the inhibitor for the last four weeks, as before. Both KHK siRNA and the inhibitor treatment reduced body weight (Figure S2E). This was accompanied by lower liver weight in the siRNA, but not in the inhibitor-treated group (Figure S2F). In fact, when normalized to body weight, the liver mass increased in the inhibitor group (Figure S2G), as it did in mice on HFD. There was no difference in the weight of epididymal adipose tissue (Figure S2H), while subcutaneous adipose tissue was lower in the inhibitor-treated mice (Figure S2I).

Small molecule inhibitor decreases ketohexokinase enzymatic activity in the liver and kidney but not in the intestine.

Due to the phenotypic differences between KHK KD and inhibition of its kinase activity, we assessed how well these modalities prevent hepatic fructose metabolism. Compared to the HFD-fed mice (549±17nM), serum fructose was elevated in HFD+Inhib treated mice (672±48nM) (Figure 2A), in line with systemic inhibition of fructose metabolism. Liver-specific KHK KD (580±31nM) did not increase serum fructose, as fructose can also be metabolized in other tissues. As expected, liver fructose concentration was higher in both HFD+siRNA (30.0±2.8nmol/g) and HFD+Inhib (27.1±3.8nmol/g) groups, compared to the HFD group (16.1±1.6nmol/g) (Figure 2B). The product of KHK activity, F1P, was reduced in the HFD+siRNA group (6.2±1.3nmol/g), compared to the HFD group (12.7±1.8nmol/g) (Figure 2C). Surprisingly, the HFD+Inhib group (29.0±10.4nmol/g) had a much higher F1P concentration 2-5 hours after the inhibitor gavage. F1P is known to induce liver injury (31), so we quantified serum ALT. The HFD group had higher ALT than the LFD group, but ALT decreased in both HFD+siRNA and HFD+Inhib groups (Figure S3A). The expression of proinflammatory genes was also increased in the HFD, compared to the LFD group, but was largely unaffected by the two interventions, except MCP1, which decreased in both HFD+siRNA and HFD+Inhib groups (Figure S3B). The expression of profibrotic genes Col1a1 and αSma was unaffected, while TGFβ increased in mice on HFD and decreased with both

interventions (Figure S3C).

Next, we calculated the F1P to fructose ratio to approximate KHK activity. The ratio was reduced only in the KHK+siRNA group, but it was unchanged in the HFD+Inhib group (Figure 2D). Hepatic KHK activity was also directly measured utilizing our recently developed protocol (32). The mice on a HFD had 23% higher KHK activity in the liver, compared to the mice on a LFD (Figure 2E). Compared to the HFD group, KD of KHK decreased KHK activity by 80%, likely reaching the background levels of the assay. However, the inhibitor lowered KHK activity by only 38%. These data agree with the F1P/Fructose ratio, confirming that the inhibitor group can still metabolize some fructose in the liver. In the kidney, only the inhibitor, but not siRNA decreased KHK activity by 36% (Figure 2F). However, in the intestine, neither intervention lowered KHK activity (Figure 2G). We compared KHK activity in the liver, intestine, and kidney to adipose tissue, which does not express KHK. In LFD-fed mice, KHK activity was 2.4-fold higher in the intestine, as compared to both the liver and kidneys (Figure 2H). Next, we measured the protein levels of total KHK and KHK-C isoform. The intestine had 3 times lower KHK-C protein compared to the liver and kidney, whereas adipose tissue didn't express KHK (Figure 2I, S4A). These data agree with a study documenting that the intestine metabolizes fructose more robustly than the liver, but can only metabolize a small amount of fructose (33). Urine fructose normalized to creatinine was two-fold higher in HFD compared to the LFD group (Figure 2J). The HFD+siRNA group did not show a further elevation; however, the HFD+Inhib group had a stepwise higher urinary fructose. Urine creatinine (Figure S4B) and urine volume collected over 24h (Figure S4C) were not different among the groups. Urine fructose excretion over 24h was higher in mice on a HFD and it further increased following both KHK KD or inhibition of its activity (Figure 2K). In summary, the KD of KHK resulted in an almost complete loss of fructose metabolism in the liver. In contrast, systemic inhibition of KHK activity partially reduced fructose metabolism in the liver and kidney, but not in the intestine.

Due to differences in KHK activity and the F1P/Fructose ratio, we tested whether the dose of the inhibitor was adequate to inhibit KHK activity *in vivo*. In a pilot study, mice were gavaged 10 mg/kg, 30 mg/kg, or 60 mg/kg of the KHK inhibitor or methylcellulose vehicle 1h before a fructose challenge test using 6 mg/kg of fructose, and blood samples were collected over time. Mice gavaged fructose and

methylcellulose had elevated serum fructose excursion over 60 min (Figure S4D). All three concentrations of the inhibitor induced a dose-dependent increase in plasma fructose levels (Figure S4D). Serum glucose (Figure S4E) and insulin (Figure S4F) were the highest in mice treated with fructose and vehicle and they decreased with the administration of 10, or 30 mg/kg of the inhibitor. Next, the level of the inhibitor in the blood was quantified over the 24h period in mice gavaged 10, or 30 mg/kg of the inhibitor. Based on *in vitro* potency, 1 μM inhibitor concentration is required to inhibit KHK activity by 90% (IC90). 10 or 30 mg/kg inhibitor dose achieved *in vivo* inhibitor concentration above the IC90 for 7-10 hours (Figure 2L). Based on these results, the mice in our experiment were given 15 mg/kg inhibitor twice daily.

The exposure to the inhibitor was measured by mass spectrometry in our experimental mice at the time of sacrifice. The pharmacokinetic model fitting profile (Figure 2M) shows the free maximum exposure of the inhibitor was 4.6 μM and the free average exposure was 1.6 μM in line with *in vitro* IC90 exposure reported by Gutierrez (23). Despite achieving the targeted plasma concentration, the inhibitor lowered KHK activity only by 38% in our study using mice, while it decreased by 90% in the Pfizer study using rats. We found that KHK protein is 4-fold more abundant in the livers of rats compared to mice (Figure S4G, S4H). On the other hand, KHK activity per μg of KHK was significantly higher in mice compared to rats (Figure S4I). The higher KHK activity in mice may explain why the inhibitor did not effectively reduce KHK function in mice, as observed in rats.

KHK siRNA specifically deletes KHK-C and increases HK2, while the inhibitor partially decreases both KHK-C and TKFC proteins.

Given the differences in target engagement, we next interrogated the fructolysis pathway (Figure 3A). The expression of enzymes catalyzing the first, second, and third steps of fructose metabolism was increased 1.3- to 2.2-fold in mice on a HFD compared to LFD (Figure 3B). KD of KHK decreased both Khk-a and Khk-c mRNA over 90% compared to the HFD group. Interestingly, inhibition of KHK activity also decreased Khk-a and Khk-c mRNA by 45-58% compared to the HFD group. KHK KD or inhibition of its activity did not affect aldolase b (Aldob) expression. The expression of the enzymes mediating the

third step of fructolysis was not affected by KHK KD, except aldehyde dehydrogenase (Aldh3a2), which was 63% higher compared to the HFD group. Conversely, inhibition of KHK activity decreased triokinase and FMN cyclase (Tkfc) expression by 40% and it increased alcohol dehydrogenase (Adh1) 1.4-fold and Aldh3a2 3.2-fold, compared to the HFD group. Similar to mRNA, KHK-C protein was increased in mice on a HFD compared to a LFD (Figure 3C, 3D). The KHK+siRNA group completely lacked KHK-C protein, whereas, interestingly, the KHK+Inhib group had 56% lower KHK-C protein. ALDOB was slightly lower in both KHK+siRNA and KHK+Inhib groups. TKFC, which catalyzes a major arm of the third step of fructose metabolism, was significantly lower in the KHK+Inhib, but not in the KHK+siRNA group. ADH1 was not different, whereas ALDH3 increased in both KHK+siRNA and KHK+Inhib groups. An unexpected decrease in TKFC protein led us to suspect that the KHK inhibitor also targets TKFC. Indeed, the KHK inhibitor is able to lower the enzymatic activity of recombinant mouse TKFC protein in a dose-dependent fashion (Figure S5A). To show that TKFC is inhibited in vivo, we quantified hepatic glyceraldehyde (GA), a substrate for TKFC (Figure S5B). GA levels were not affected (Figure S5C), but its metabolite, glycerate (Figure S5D) as well as 3-phosphoglycerate (Figure S5C) were upregulated. This agrees with elevated aldehyde dehydrogenase in the KHK+Inhib group and provides indirect evidence that TKFC is inhibited in vivo. Together, these data indicate that KHK siRNA profoundly decreased KHK-C mRNA and protein, while KHK inhibitor decreased protein and enzymatic activity of both KHK-C and TKFC.

In the absence of KHK, fructose may be metabolized by an alternative pathway where hexokinase (HK) phosphorylates fructose to fructose-6 phosphate (F6P). There are four hexokinases, one, two, three, and four, a.k.a. Gck. The HFD+siRNA group showed an increase in HK2 mRNA (Figure S5B) and protein levels (Figure 3E, 3F) consistent with an alternate route of fructose metabolism. On the other hand, HK1, HK2, and HK3 were lower in the HFD+Inhibit treated mice since they had partially preserved KHK activity (Figure 2E), and GCK activity was elevated in this group (Figure S2D). The expression of hexokinases is much lower than Gck in the liver (Figure 3G). However, fasted fructose concentration (0.01 mM)(34) is also much lower than glucose (5 mM), so low abundance of HK2 may still play a physiologic role in the HFD+siRNA treated mice. An increase in all three steps of fructose metabolism in mice on a HFD can be explained, in part, by endogenous fructose

production mediated by aldo-keto reductase (Akr1b1) and sorbitol dehydrogenase (Sord), which were increased in all mice on a HFD (Figure 3H). In summary, KHK KD more completely abolished KHK activity, leading to alternative metabolism via HK2. Conversely, the KHK inhibitor partially lowered both KHK-C and TKFC activities, which may account for increased F1P in this group.

Knockdown of ketohexokinase, but not inhibition of its kinase activity, improves glucose tolerance.

The mice on a HFD had impaired glucose tolerance compared to the LFD-fed mice (Figure 4A, 4B). KHK KD improved glucose tolerance, but inhibition of KHK kinase activity did not. Similarly, fasted blood glucose was elevated in mice on a HFD (171±9mg/dL) compared to the LFD group (132±3mg/dL) (Figure 4C). Glucose levels improved in the KHK siRNA (138±5mg/dL), but not the inhibitor group (157±6mg/dL). Fasted insulin was higher in the HFD (2.0±0.2ng/ml) compared to the LFD group (0.3±0.1ng/ml), and was reduced after both KHK KD (0.9±0.1ng/ml) and the inhibitor treatment (0.8±0.1ng/ml) (Figure 4D). Similarly, HOMA-IR, a measure of whole-body insulin resistance, was elevated in mice on a HFD and was decreased in both KD and inhibitor arms (Figure 4E). Insulin-stimulated Akt phosphorylation was lower in mice on HFD compared to the LFD group (Figure 4F, S6A). KD of KHK or inhibition of its activity improved Akt phosphorylation. Erk phosphorylation was also decreased in the HFD compared to the LFD group, but it did not improve with KD or inhibition of KHK. Thus, improved glucose tolerance following KHK KD is not due to improved hepatic insulin signaling, which was equally better after both KHK KD or inhibition.

Glyceraldehyde-3-phosphate dehydrogenase (GAPDH) controls the flow of fructose carbons onto the glycolysis pathway. GAPDH was slightly increased in the HFD- compared to the LFD-fed mice (Figure 4G, S6B). KHK KD profoundly lowered GAPDH, in agreement with the abrogation of fructose metabolism. Inhibition of KHK activity did not lower GAPDH. The rate limiting enzyme of glycolysis, phosphofructokinase (PFK), was decreased in the HFD group, compared to the LFD group (Figure 4G, S6B). The mice in the HFD+siKHK group, but not in the HFD+Inhib group, had elevated PFK protein. The last enzyme of glycolysis, pyruvate kinase (PK) is allosterically activated by fructose-1,6-

bisphosphate, the product of PFK activity. Therefore, PK was elevated in the HFD+siRNA group, compared to the HFD+inhib group. Pyruvate dehydrogenase (PDH) converts pyruvate into acetyl-CoA. PDH was unchanged among the groups. Next, we assessed the gluconeogenesis pathway by qPCR. Gapdh mediates both the fructolysis and gluconeogenesis pathways. Gapdh mRNA mimicked its protein, which likely reflects its role in fructolysis (Figure 4H). All other enzymes of gluconeogenesis, phosphoenolpyruvate carboxykinase 1 (Pck1), enolase (Eno1), phosphoglycerate kinase 1 (Pgk1), fructose-bisphosphatase 1 (Fbp1) and glucose-6-phosphatase (G6pc1) were not different between the HFD+siKHK and HFD+Inhib groups. Together, these data demonstrate that glucose handling is differentially regulated by KHK KD or inhibition of its kinase activity.

To further investigate the differences in glucose handling, we performed mass spectrometry analysis and quantified 880 hepatic metabolites. KHK KD or inhibition of its kinase activity profoundly altered hepatic metabolome on principle component analysis (Figure S7A). A heatmap representation of the top 110 metabolites showed that the HFD+Inhib group had an increase in acetyl-CoA and coenzyme A, substrates for DNL (Figure S7B). On the other hand, the HFD+siRNA group had an increase in mono and polyunsaturated fatty acids, such as 9-decenoic acid and adrenic acid (Figure S7B). Given that the most abundant changes occurred in hepatic lipids, next, we focused on metabolites in the FAO pathway. The HFD+Inhib group had an increase in carnitine and acetylcarnitine (Figure 4I, S8), while long-chain acylcarnitines, such as palmitoylcarnitine and stearoylcarnitine were increased in the HFD+siRNA compared to the HFD+Inhib group (Figure 4J, S8). An increase in short-chain and a decrease in long-chain acylcarnitines is indicative of enhanced FAO in the HFD+Inhib group. In summary, the hepatic metabolome was profoundly different following KHK knockdown versus KHK inhibition. This difference is largely driven by the alterations in hepatic lipid handling.

RNAseq analysis reveals profound and unique roles of ketohexokinase knockdown versus inhibition on hepatic transcriptome

We assessed global gene expression in these mice by RNAseq. The principal component analysis revealed that gene expression in the HFD group clustered differently than in the LFD group

(Figure 5A). Following KHK KD, the gene expression clustered between the LFD and HFD groups, while KHK inhibition dramatically altered hepatic gene expression in a new direction. A heatmap analysis of the top 40 genes identified a unique pattern of gene expression among the groups (Figure 5B). Some of the genes that were upregulated in HFD and decreased by both KHK KD and inhibition are involved in the regulation of cholesterol, such as Apoe4 and the formation of atherosclerotic plaques, such as matrix metalloproteinase 12 (Mmp12). The genes that were decreased in HFD and restored by both KHK siRNA and inhibitor treatment are involved in ribosomal function, such as ribosomal protein S3 (Rps3) and ribosomal protein lateral stalk subunit P0 (RPLP0). The genes that were lowered by KHK KD, but not by the inhibitor treatment regulate lipid assemble, such as lysophosphatidylglycerol acyltransferase 1 (Lgpat1) and glycerol kinase (Gk). The genes that were normalized by the inhibitor, but not by KHK siRNA treatment were members of proteoglycans, such as glypican 1 (Gpc1) and proteoglycan 4 (Prg4). Interestingly, a number of genes regulating FAO were increased uniquely in the inhibitor group, such as acyl-CoA thioesterase 2 (Acot2) and acyl-CoA oxidase 1 (Acox1), in agreement with our metabolomics analysis. Next, we honed in on the differentially regulated pathways. The expression of the DNL pathway, regulated by transcription factor carbohydrate-responsive element-binding protein (ChREBP), was profoundly downregulated by KHK siRNA treatment (Figure 5C). On the other hand, KHK inhibition led to upregulation of the FAO pathway, regulated by the peroxisome proliferator-activated receptor alpha (PPARα) transcription factor (Figure 5D).

Volcano plot comparison of the individual groups revealed that the upregulated genes in the HFD, compared to the LFD group are involved in lipid homeostasis, including Gk, Apoa4 and 3-hydroxybutyrate dehydrogenase 1 (Bdh1) (Figure 5E). The most downregulated genes in the KHK siRNA group, compared to the HFD group, were the genes involved in fructose metabolism, Khk and Gapdh, but also the genes involved in fatty acid synthesis, such as stearoyl-CoA desaturase 1 (Scd1), and acetyl-CoA carboxylase (Acc2) (Figure 5F). The genes increased with the inhibitor treatment, compared to the HFD group, are involved in lipid oxidation, including Acot2, Acox1 and enoyl-CoA hydratase and 3-hydroxyacyl CoA dehydrogenase (Ehahdh) (Figure 5G). These same genes were

upregulated in the KHK+Inhib group compared to the HFD+siRNA group, as they were uniquely upregulated by the inhibitor treatment (Figure 5H). Reactome pathway analysis revealed that some of the most downregulated pathways in the HFD+siRNA group mediate carbohydrate metabolism and de novo synthesis of lipids, such as sphingolipids (Figure 5I). Conversely, some of the most upregulated pathways in the HFD+Inhib group were mediating mitochondrial and peroxisomal FAO (Figure 5J). These changes persisted when the HFD+Inhib was compared to the HFD+siRNA group (Figure S9A).

An increase in FAO pathway and PPARα target genes with the inhibitor treatment was unexpected, so we assessed PPARα expression, which was elevated in the HFD and KHK+siRNA groups and was stepwise higher in the HFD+Inhib group (Figure S9B). Next, we tested whether the inhibitor or F1P, produced by the inhibitor treatment, can bind to PPARα ligand binding domain to increase PPARα transcriptional activity in COS-7 cells transfected with PPARα luciferase reporter. As expected, WY14643, a PPARα agonist, increased luciferase activity in a dose-dependent fashion (Figure S9C); however, neither the inhibitor (Figure S9D) nor F1P (Figure S9E) increased PPARα luciferase activity. Next, we performed kinase activity measures in real-time for serine/threonine kinases (STK) and phospho-tyrosine kinases (PTK) using PamGene PamStation microarray PamChip technology. Some of the most upregulated STKs in the HFD+siRNA, compared to the HFD group, were AKT1 and AKT2 in line with improved glucose tolerance in this group (Figure S10A). Conversely, the most downregulated STK in the HFD+Inhib, compared to the HFD group, was glycogen synthase kinase 3 beta (GSK3β) (Figure S10B). Lower GSK3β activity in the HFD+Inhib group may explain PPARα activation in this group, since GSK3β phosphorylates and deactivate PPARα.(35) Moreover, reduced GSK3β activity aligns with increased glycogen accumulation in this group, as GSK3β phosphorylates and deactivates GYS (36). There was no difference in PTK activity between KHK KD or inhibition (Figure S10C, S10D). In summary, KHK KD primarily lowered the DNL pathway, while the inhibitor treatment increased the FAO pathway.

Ketohexokinase knockdown decreased DNL, while the inhibitor increased the FAO pathway.

We verified some of the most interesting changes in RNAseq data by qPCR and Western blot.

ChREBP-β (MLXIPL-β), the active isoform of ChREBP transcription factor, was decreased in all mice on HFD, compared to the LFD group (Figure 6A), since the HFD contains fewer carbohydrates. MLXIPL-β, was further reduced with the siRNA, but not in the inhibitor group (Figure 6A). The expression of MLXIPL-α tended to be reduced in all mice on HFD (Figure S11A). The expression of sterol regulatory element-binding transcription factor 1c (SREBF1c) was elevated two-fold in all mice on HFD, compared to the LFD group, but there was no further effect with siRNA or the inhibitor treatment (Figure 6B). SREBF1a followed a similar expression pattern (Figure S11B). Nuclear translocation of ChREBP was similar in mice on HFD and LFD (Figure 6C, S11C). KHK siRNA decreased ChREBP compared to the HFD group. The inhibitor treatment did not significantly lower ChREBP translocation when normalized to lamin. Nuclear translocation of SREBP1 was higher in mice on a HFD, compared to the LFD group (Figure 6C, S11D). SREBP1 was not markedly affected in the HFD+siRNA and HFD+Inhib groups. The expression of downstream genes mediating lipogenesis was not elevated in mice on a HFD, but they were profoundly reduced in the HFD+siRNA, and not in the HFD+Inhib group (Figure 6D), consistent with the changes in ChREBP. The protein levels of these lipogenic enzymes were likewise profoundly decreased only in the HFD+siRNA group (Figure 6E, S11E).

Next, we quantified the protein levels of the enzymes mediating mitochondrial beta-oxidation. CPT1α, the rate-limiting enzyme of mitochondrial FAO, was increased in the HFD group compared to the LFD group (Figure 6F, S11F). CPT1α was further elevated in the HFD+siRNA, but not in the HFD+Inhib group. The protein levels of ACADVL, ACADL, and HADHA were not significantly affected. However, mRNA expression of these genes was significantly elevated in mice on a HFD and they further increased in the HFD+Inhib, but not in the HFD+siRNA group (Figure 6G). The protein levels of enzymes mediating peroxisomal FOA were markedly elevated 2 to 240-fold only in the HFD+Inhib group (Figure 6H, S11G) and their mRNA expression was 4 to 20-fold higher compared to the LFD group (Figure 6I). The expression of genes mediating fatty acid transport into the liver, CD36, Fatp2, and L-Fabp were also profoundly elevated in the HFD+Inhib group (Figure S11H). In summary, KHK KD markedly decreased the DNL pathway, whereas the KHK inhibitor profoundly increased the FAO pathway, in agreement with RNAseq data.

In vitro overexpression of wild-type, but not mutant kinase-dead KHK increases hepatocyte injury and glycogen accumulation.

The differences between KHK KD and inhibition of its kinase activity may be secondary to the kinase-independent functions of KHK. We overexpressed GFP-tagged wild-type mouse KHK-C (WT) or kinase-dead mutant KHK-C (KM) in human HepG2 cells using lentivirus to test this hypothesis. KM KHK-C was generated by introducing a point mutation (G527R) in the ATP binding domain. For comparison, the KHK inhibitor similarly targets the ATP binding domain. Compared to the HepG2 control cells (CC), overexpression of both WT or KM robustly induced mouse KHK-C expression (Figure 7A). KHK-C protein was much higher in the cells overexpressing WT, compared to KM, suggesting lower protein stability (Figure 7B). Indeed, when treated with cycloheximide, a protein synthesis inhibitor, KM KHK-C protein degraded faster than WT KHK-C protein (Figure S12A). KHK enzymatic activity was markedly elevated in WT KHK-C cells but not in KM KHK-C cells treated with fructose, confirming that the kinase-dead mutant isn't able to metabolize fructose (Figure 7C). Increased KHK activity in cells that do not express downstream ALDOB or TKFC (Figure 7B, S12B) is expected to lead to the accumulation of F1P. Thus, WT KHK-C cells treated with 5mM fructose, but not glucose, exhibit higher cell injury manifested by elevated alanine aminotransferase (ALT) in cell supernatant (Figure 7D). Cell injury can lead to hepatocyte loss and we saw lower total protein in WT KHK-C cells treated with fructose, but not 3-O methylfructose (3-OMF), a non-metabolizable analog of fructose (Figure 7E). ALT and protein levels were not affected in KM cells.

Similar to *in vivo* findings, PAS glycogen staining was higher in fructose-treated WT, but not KM or CC cells (Figure 7F). Indeed, glycogen levels were increased with fructose compared to glucose treatment in all cells, but were the highest in the WT KHK-C cells (38.9±2.0ng/ug), compared to CC (19.9±0.2ng/ug) or KM (15.2±0.5ng/ug) cells (Figure 7G). HepG2 cells don't express Gck, however Gckrp was increased over 2-fold in WT KHK-C cells and it completely normalized following fructose, but not 3-OMF treatment (Figure 7H). In the absence of Gck, Gckrp may regulate hexokinase activity and expression. Indeed, Hk1 expression was 5-fold higher in WT KHK-C cells treated with fructose (Figure

7I). Hk2 expression was not affected by fructose or 3-OMF treatment (Figure 7J). In agreement with mRNA, GCK protein was not abundant in HepG2 cells compared to mouse liver (Figure 7K, S12C). HK1 protein was only elevated in WT KHK-C cells, whereas HK-2 was increased 2-3 fold in both WT and KM cells (Figure 7K, S12D). HK3 was not altered, while GAPDH tended to be higher in both WT and KM cell.

Lastly, we interrogated DNL and FAO pathways. Fructose-treated WT KHK-C cells did not increase Acly, Acc1, Fasn, or Scd1 expression (Figure 7L). Interestingly, the cells overexpressing KM KHK-C had significantly higher expression of DNL enzymes. This suggests that the DNL pathway is, in part, regulated through the kinase-independent function of KHK-C. This correlated with increased expression of ChREBF and SREBP1c in KM but not WT cells (Figure S12E, F). Conversely, fructose-fed WT, but not KM, KHK-C cells had decreased expression of genes regulating FAO (Figure 7M). These data indicate that fructose metabolism and thus KHK activity is required to decrease FAO. In summary, KHK activity is required to generate F1P, induce glycogen accumulation and decrease FAO, whereas DNL is independent of KHK-C kinase function.

DISCUSSION

In this work, we examined the impact of liver-specific knockdown of KHK versus systemic inhibition of KHK kinase activity. These two approaches targeting the same enzyme exert uniquely different metabolic outcomes. KHK siRNA completely and specifically deletes KHK protein in the liver. This leads to the upregulation of an alternative pathway of fructose metabolism via HK2, and improves glucose tolerance. Conversely, KHK inhibitor targets both KHK and TKFC proteins, resulting in F1P accumulation in the liver. Elevated F1P is associated with glycogen accumulation, hepatomegaly, and impaired glucose tolerance. Perhaps the most striking difference between KHK KD and inhibition is in the regulation of hepatic gene expression. KHK KD profoundly decreases the expression of genes in the DNL pathway, which is not observed following the inhibition of its kinase activity. Similarly, overexpression of kinase-dead mutant KHK-C increases the expression of DNL genes suggesting kinase independent role. On the other hand, the KHK inhibitor uniquely upregulates the expression of PPARα target genes and alters hepatic metabolome in favor of elevated FAO. In conclusion, liver-specific KHK KD exerts beneficial effects on hepatic metabolism, while the inhibitor increases glycogen buildup via its off-target effect on TKFC. Therefore, siRNA-mediated KD of KHK may offer important advantages over the KHK inhibitor.

Liver-specific KHK KD induces a more complete abrogation of fructose metabolism, evident by minimal KHK activity, lower hepatic F1P/Fructose ratio, and activation of an alternative pathway of fructolysis via HK2. In spite of achieving adequate plasma IC90 concentration, fructose metabolism in the liver is only partially reduced by the inhibitor, as indicated by an incomplete reduction of KHK activity, normal F1P/Fructose ratio, and no improvement in systemic glucose tolerance. The F1P/Fructose ratio is higher in the inhibitor-treated mice than expected, given that partial inhibition of KHK activity should reduce fructolysis and, thus, F1P levels. Instead, F1P concentration was the highest in the HFD+Inhib group, which could be explained by lower TKFC activity. Consistent with this interpretation, Liu et al., reported increased F1P in primary hepatocytes treated with TKFC shRNA and fructose avoidance in TKFC KO mice (37). A reduction in both KHK and TKFC activity may be due to the inhibitor targeting the ATP binding domain of these two enzymes. KHK and TKFC are the only kinases within the first three

steps of fructose metabolism and thus possess ATP binding domain. Indeed, we show direct evidence that the KHK inhibitor is able to lower the enzymatic activity of recombinant mouse TKFC protein. We also show increased degradation of KHK-C protein harboring kinase inactivating mutation. A decrease in KHK and TKFC proteins could also be due to reduced ChREBP transcription of these enzymes. Contrary to this possibility, ChREBP is actually lower following KHK KD than with the inhibitor treatment. Taken together, these data implicate that the off-target effects of the KHK inhibitor on TKFC may, in part, explain F1P buildup and glycogen accumulation in the inhibitor-treated mice.

F1P is a toxic metabolite that leads to hepatic glycogen accumulation and hepatocellular injury (38). Cytotoxic properties of F1P have been documented from yeast (39), to human cells (40). We observe higher ALT and lower total protein in fructose-treated cells expressing wild-type KHK-C. Moreover, we also see increased glycogen accumulation in the livers of mice with elevated F1P and in fructose-treated cells overexpressing wild-type KHK-C. Glycogen accumulation in the HFD+Inhib treated mice can be accounted for by several mechanisms. Glucokinase is bound by glucokinase regulatory protein that inhibits its activity (41). F1P promotes the dissociation of the complex and allows the production of substrates for glycogenesis (42). Additionally, F1P increases the activity of glycogen synthase (43). Another explanation for higher glycogen accumulation is a decrease in serum glucagon. These processes are interrelated as glucagon plays a role in regulating F1P levels (44).

The strong propensity of F1P to stimulate glycogen accumulation is observed in the cells that overexpress wild-type, but not kinase-dead KHK. These cells also lack ALDOB required for further metabolism of F1P. *In vitro*, fructose metabolism decreases Gckrp expression and leads to upregulation of hexokinase 1, which may provide a substrate for glycogen synthesis. Indeed, a dual role of F1P to support glycogenesis and induce hepatotoxicity is best observed in patients with hereditary fructose intolerance (HFI) due to ALDOB deficiency (38). The symptoms of HFI can be completely avoided in mice lacking KHK in order to prevent fructose metabolism to F1P (45). Interestingly, in our study, an increase in F1P following the inhibitor treatment induced glycogen accumulation, but was not associated with increased liver injury or inflammation.

Both KD of KHK and inhibition of its kinase activity effectively resolve hepatic steatosis. However, these modalities reduce hepatic fat accumulation via substantially different mechanisms. RNAseq analysis reveals that a complete absence of KHK protein, but not inhibition of its kinase activity decreases the expression of genes mediating DNL. This is confirmed by markedly lower mRNA and protein levels of DNL enzymes, ACLY, ACC1, FASN, and SCD1 in the HFD+siRNA, but not the HFD+Inhib group. The effects on the DNL pathway are likely mediated by kinase independent effects of KHK, as overexpression of kinase-dead mutant KHK was sufficient to increase the mRNA of DNL genes. We recently reported the first evidence pointing to kinase independent effects of KHK in mediating protein acetylation (28). Acetylated proteins may not fold properly, triggering misfolded protein response and endoplasmic reticulum (ER) stress. Indeed, we reported that KHK drives ER stress, a function that is independent of fructose metabolism (29). Alternatively, the effects of KHK on the DNL pathway may be, in part, mediated by a greater reduction in ChREBP. Indeed, histone acetylation is a powerful mode of regulating gene expression and acetylation of ChREBP increases its activity (46). Unlike our results, the KHK inhibitor has been reported to reduce DNL in rats (23). We may not have observed a decrease in the DNL pathway with the inhibitor treatment as we did not use a diet high in fructose, we achieved only 38% inhibition of KHK in the liver, and mice are less sensitive to the effects of dietary fructose than rats. Most of our studies were preformed using a HFD, as this is the most common diet-induced obesity method, and a potential treatment for MASLD would ideally work for all patients, not only the ones consuming high amounts of fructose.

While KHK KD lowers the DNL pathway, the small molecule inhibitor uniquely and profoundly increases the expression of genes regulating FAO. Metabolomics analysis confirmed that the HFD+Inhib group had increased levels of short-chain and a decrease in long-chain acylcarnitines. Enhanced FAO pathway is not mediated by direct binding of the inhibitor to the PPARα ligand binding domain. However, lower GSK3β activity in the inhibitor group could activate the FAO pathway, as GSK3β has been reported to phosphorylate and inhibit PPARα (35). PPARα activation could also, in part, explain hepatomegaly in the HFD+Inhib group as increased PPARα activity leads to hepatocyte proliferation (47). Moreover, PPARα activation explains an increase in cholesterol (48), which in mice mainly consists of HDL

cholesterol. Lastly, PPARα activation may account for lower serum glucagon since keto acids decrease glucagon secretion (49). In addition to PPARα activation, another mechanism for the enhanced FAO pathway is a decrease in TKFC. A knockout of TKFC in the liver shifts the third step of fructose metabolism toward the ALDH pathway resulting in increased FAO (37). In our study, ALDH was indeed more strongly upregulated in the HFD+Inhib, than in the HFD+siRNA group. The inhibitor-induced upregulation of the FAO pathway may explain lower steatosis without a substantial decrease in the DNL pathway.

Fructose intake is a well-recognized risk factor for the development of obesity and metabolic dysfunction. We show that targeting KHK via liver-specific siRNA completely and specifically prevents fructose metabolism and results in the resolution of hepatic steatosis and improves glucose tolerance. On the contrary, a small molecule inhibitor of KHK only partially reduces KHK activity in the liver, but it also targets TKFC, resulting in elevated F1P, glycogen accumulation, hepatomegaly, and no improvement in glucose tolerance. Our study reaffirms that targeting KHK is still a viable option for the management of metabolic dysfunction in spite of the discontinuation of the KHK inhibitor from further clinical development. Based, in part, on the results of this study our collaborators at Alnylam completed phase 1 and are progressing with a phase 2 clinical trial (NCT05761301) testing KHK siRNA in subjects with obesity and diabetes.

METHODS

Sex as a biological variable. Our study exclusively examined male mice as female mice do not develop profound obesity and fatty liver disease. It is unknown whether our findings are relevant to female mice.

Animals and Diets

Mice were housed at 20-22 ºC on a 12 h light/dark cycle with *ad libitum* access to food and water. C57Bl/6J male mice at 6 weeks of age were purchased from Jackson Laboratory and fed either a low-fat diet (LFD, Research Diets D12450K) or a 60% high-fat diet (HFD, Research Diets, D12492) for 6 weeks. Thereafter, the mice on a high-fat diet were subdivided into three groups: the control group (HFD), the KHK siRNA group (HFD+siRNA), and the KHK inhibitor group (HFD+Inhib). To ensure equal stress/treatment, all mice were injected with either luciferase control siRNA (10 mg/kg) or siRNA targeting total KHK (20 mg/kg) every two weeks and were gavaged either methylcellulose control or (15mg/kg) KHK inhibitor (PF-06835919) in methylcellulose, twice daily for four weeks. The animals were weighed, and their food intake was recorded once per week. GTT and ITT were performed after 8 and 9 weeks of feeding, respectively. The mice were sacrificed after 10 weeks on the diet. The mice were injected saline or 1U of insulin (Humulin R-Lilly #HI-213) via inferior vena cava 10 minutes before tissue collection in liquid nitrogen.

Liver-specific KHK knockdown

Liver-specific knockdown was achieved by utilizing an siRNA conjugated to N-acetylgalactosamine (GalNAc). Alnylam Pharmaceuticals synthesized siRNA to specifically target mouse total Khk mRNA. siRNA has undergone chemical modifications to achieve long-lasting effect and specificity for hepatocytes. The guide strand is conjugated to a trivalent GalNAc specifically recognized by the asialoglycoprotein receptor (ASGPR), which is highly expressed on the surface of hepatocytes, achieving hepatocyte-specific delivery and uptake.

KHK inhibitor dose calculations and pharmacokinetic studies

KHK inhibitor, PF-06835919 was synthesized at Pharmaron based on the structure of described in (50). The *in vitro* potency, 5 nM, of the compound was confirmed using the method described in (32). The compound was formulated in 0.5% HPMC 10000 cP, 0.1% Tween80, pH 9.

Male c57bl/6J mice on 60 % HFD (Research Diets D12492) starting at 6 weeks age, were purchased at 16 weeks of age from Taconic Denmark and kept in an Association for Assessment and Accreditation of Laboratory Animal Care (AAALAC) accredited facility. Prior to the fructose tolerance test, the mice were gavaged 10 mg/kg, 30 mg/kg or 60 mg/kg of the KHK inhibitor or methylcellulose vehicle. One hour later, 6 mg/kg of fructose or water was gavaged and repeated blood samples were collected over 1h. Fructose was analyzed using BioAssay Systems EnzyChrom™ Fructose assay Kit (EFRU-100), glucose was measured using ACCU-chek device, and insulin was measured by ELISA (Chrystal Chem Ultra Sensitive Mouse Insulin ELISA Kit (Cat # 90080).

In vivo inhibitor concentration: Plasma was collected for exposure analysis at the termination of the main experiment. The plasma samples were precipitated with 100% acetonitrile. After vortexing and centrifugation the supernatant was transferred to a new plate and diluted 1:2 with H_2O, 0.2% formic acid. Matrix-matched calibration samples, quality controls for PF-06835919, and blanks were prepared in the same way as the study samples. The samples were injected on an Acquity Ultra Performance LC coupled to a Sciex API 4500 mass spectrometer. The mass spectrometry method was operated in positive electrospray mode using multiple reaction monitoring of transitions 357.2 >315.3 for PF-068359198. Plasma concentration of PF-06835919 was measured from 2 to 5 hours after the last dose. Therefore, we fitted these data with 1 compartmental pharmacokinetic model to assess if the average plasma concentration was in line with the predicted target exposure.

Glucose and insulin tolerance test

For glucose tolerance test (GTT), mice were fasted overnight and injected intraperitoneally (IP) with 2g glucose per kg of body mass. Blood glucose levels were measured at 0, 15, 30, 60, and 120

minutes using a glucose meter (Infinity, US Diagnostics). Insulin tolerance tests (ITT) were performed in nonfasted mice by i.p. injection of 1 mU insulin per kg of body mass. Blood glucose levels were measured at indicated times.

Liver Histology and serum assays

The slides were prepared from formalin-fixed, paraffin-embedded liver sections. H&E staining and Periodic acid–Schiff staining were performed by the University of Kentucky Pathology Research Core. Liver homogenates were used for the quantification of triglycerides (Pointer scientific, T7532-1L) following the manufacturer's guidelines, as previously published (51). Plasma insulin was quantified using an ELISA kit (Crystal chem, 90080). ALT levels were measured using commercial ALT kit (Catachem, C164-0A). Urinary fructose was quantified using a fructose assay kit (BioAssay Systems, EFRU-100).

qPCR and mRNA quantification

Gene expression was quantified as previously described (52). Briefly, mRNA was extracted by homogenizing liver tissue in trizol, treating with chloroform and participating in 70% ethanol. mRNA was purified using RNeasy Mini Kit columns (Qiagen, #74106). cDNA was made using High Capacity cDNA Revers Transcription Kit (Applied Biosystems, #4368813). qPCR was performed utilizing C1000 Thermal Cycler (BioRad, CFX384) and QuantStudio™ 7 Flex Real-Time PCR System (TermoFisher Scientific, 4485701). Mouse and human primer sequences are listed in the Supplemental tables 1 and 2, respectively. An average of 18S and TBP was used to normalize the mRNA data.

Protein Extraction and Immunoblot

Tissues were homogenized in RIPA buffer (EMD Millipore) with protease and phosphatase inhibitor cocktail (Bimake.com, B14002, B15002). 10 – 20 ug of protein were loaded on the gel. Proteins were separated using SDS-PAGE gel and transferred to the PVDF membrane (Millipore). Immunoblotting was achieved using the indicated antibodies listed in the Supplemental table 3. Images

were captured by ChemiDoc MP imaging system (BioRad, 12003154) and iBright imaging system (Thermo Fisher, CL1000). Quantification of immunoblots was performed using ImageJ.

KHK and TKFC activity assays

KHK activity was measured with luminescence-based method as previously published (32). TKFC activity was measured using mouse recombinant TKFC protein (Origene, TP509059). The assay measures ADP production in a reaction where D-glyceraldehyde (GA) and ATP are converted by D-glyceraldehyde-3Phospate and ADP. Recombinant TKFC protein was preincubated with KHK inhibitor or vehicle control for 15 min at 37 °C. Thereafter, the mixture was added to the reaction containing 100 mM Tris-HCl, 5 mM MgCl2, 200 uM ATP, and 0.1 mg/ml bovine serum albumin at pH 7.5 and incubated for 5 min at RT. Then, 0.5 mM GA was added and incubated for an additional 60 min at 37 °C. ATP consumption was measured using an ADP glo kit (Promega, PAV6930).

Generation of Stable KHK-C Overexpressing HepG2 cells

HepG2 cells were purchased from American Type Culture Collection (ATCC) and cultured under standard conditions in 1:1 DMEM and Ham's F-12 media (Corning) supplemented with 10% fetal bovine serum and 1% penicillin-streptomycin. Lentiviral particles were purchased from Origene containing the mouse KHK-C sequence (MR204149L2V) or Kinase dead mutated KHK-C fused to GFP (custom ordered, Origene). HepG2 cells were transduced with lentivirus at a MOI of 5 and media was changed every two days. After 5 days, GFP+ cells were sorted and propagated for an additional 2-3 weeks. KHK-C was quantified by both QPCR and western blot.

Matrix-Assisted Laser Desorption/Ionization Mass Spectrometry Imaging of Glycogen In Situ

MALDI imaging of in situ glycogen was performed based on the previously described technique (53). Formalin-fixed paraffin embedded (FFPE) tissues or purified glycogen were sectioned at 5 µm or spotted directly onto glass slides. The slide went through dewaxing and rehydration washes, followed by antigen retrieval in a citraconic anhydride buffer solution. An HTX M5 robotic sprayer was used to coat tissues in a solution of isoamylase. Following the application of enzyme, the slides were incubated

for 2 hours at 37^0C in a humidity chamber, then dried overnight in a vacuum desiccator. The following day, the robotic sprayer coated the slides with a 7 mg/mL CHCA matrix and the slides were stored in a desiccator until MALDI-MSI analysis. The slides were loaded into a Waters Synapt G2 SX mass spectrometer that used a UV laser of 100 µm in size to detect N-glycans and glycogen. Data analysis was then performed using Waters High Definition Imaging (HDI) software.

RNA Sequence Analysis and Bioinformatics Methods

HTG EdgeSeq mRNA sequence analysis was performed by the BioPolymers Facility at Harvard Medical School. Bioinformatics analysis was performed as we previously published (54).

PPARα Transcriptional Activity Assay -See Supplemental Table 5

Metabolomics and kinome analysis -See Supplemental Table 5

Statistical Analyses

All data are presented as the mean ± SEM. The data analysis, comparing the effects of control to experimental conditions was first analyzed using one-way analysis of variance (ANOVA) with Dunnett's multiple comparisons test for comparison of the individual groups. Significant differences among control and experimental groups are noted with a number sign (#), and significant differences between the individual groups under a black line are indicated by an asterisk (*). For both signs, a single symbol represents a p-value of <0.05; two symbols represent a p-value of <0.01; three symbols denote a p-value of <0.001, and four symbols represent a p-value of <0.0001 throughout the study.

Study Approval

All animal protocols were in accordance with the NIH guidelines and were approved by the IACUC of the University of Kentucky. Pilot fructose tolerance test: The experimental procedures were approved by the Gothenburg, Sweden ethics review committee on animal experiments (2002-2019).

Data availability statement

The RNA-Seq data sets can be accessed from GEO with accession ID GSE278322. Metabolomics analysis is included in Supplemental table 4. Values for all data points shown in graphs can be found in the Supporting Data Values file.

AUTHOR CONTRIBUTIONS

Conceptualization, S.H.P., S.S.; Methodology, L.R.C., H.C, R.C.S., K.W., G.O., J.B., T.D.H.; Formal Analysis, L.R.C., R.C.S., Z.A.K., E.A.B, S.J., C.J.; Investigation, S.H.P., T.F., L.R.C., H.C., R.C.S., K.W., J.B. G.O., A.B., M.P., S.J., A.S.L, C.J., Z.A.K., E.A.B T.D.H., G.J.M.; Resources, K.W., G.O., J.B., S.D., T.D.H., C.J.; Data Curation, L.R.C., R.C.S., Z.A.K., E.A.B, S.J.; Writing – Original Draft, S.H.P., S.S.; Supervision, S.S.; Project Administration, S.H.P., T.F., S.S.; and Funding Acquisition, S.S.

FUNDING

This work was supported in part by the NASPGHAN Foundation Young Investigator Award, Pediatric Scientist Development Program Award (HD000850) and the COCVD Pilot and Feasibility Grant (GM127211) awarded to SS. Alnylam Pharmaceutical funded this work, in part, via a sponsored research agreement awarded to SS. This research was supported by the University of Kentucky Office of the Vice President for Research through the Diabetes and Obesity Research Priority Area.

ACKNOWLEDGEMENT

The authors would like to thank Leila Noetzli, Ho-Chou Tu, and Kevin Fitzgerald at Alnylam Pharmaceutical for their assistance with the project. Additionally, we thank Mark Keibler for quantifying F1P *in vivo*. We greatly appreciate Terry Flier and Anna Borodovsky at Alnylam for critically reading the manuscript. Next, we would like to thank Jian-Ming Liu for measuring the *in vitro* potency of the inhibitor and Sara Lindblom for formulating the inhibitor for oral administration at AstraZeneca. We thank Gregory Graft for providing ABCD2 antibody. We thank the BPF Genomics Core Facility at Harvard Medical School for their expertise and instrument availability that supported RNAseq work.

REFERENCES

1. Nishida C, Uauy R, Kumanyika S, and Shetty P. The joint WHO/FAO expert consultation on diet, nutrition and the prevention of chronic diseases: process, product and policy implications. *Public Health Nutr.* 2004;7(1A):245-50.
2. Johnson RK, Appel LJ, Brands M, Howard BV, Lefevre M, Lustig RH, et al. Dietary sugars intake and cardiovascular health: a scientific statement from the American Heart Association. *Circulation.* 2009;120(11):1011-20.
3. Canadian Diabetes Association Clinical Practice Guidelines Expert C, Dworatzek PD, Arcudi K, Gougeon R, Husein N, Sievenpiper JL, et al. Nutrition therapy. *Can J Diabetes.* 2013;37 Suppl 1:S45-55.
4. European Association for the Study of the L, European Association for the Study of D, and European Association for the Study of O. EASL-EASD-EASO Clinical Practice Guidelines for the Management of Non-Alcoholic Fatty Liver Disease. *Obes Facts.* 2016;9(2):65-90.
5. Softic S, and Kahn CR. Fatty liver disease: is it nonalcoholic fatty liver disease or obesity-associated fatty liver disease? *Eur J Gastroenterol Hepatol.* 2019;31(1):143.
6. Softic S, Cohen DE, and Kahn CR. Role of Dietary Fructose and Hepatic De Novo Lipogenesis in Fatty Liver Disease. *Dig Dis Sci.* 2016;61(5):1282-93.
7. Softic S, Gupta MK, Wang GX, Fujisaka S, O'Neill BT, Rao TN, et al. Divergent effects of glucose and fructose on hepatic lipogenesis and insulin signaling. *J Clin Invest.* 2017;127(11):4059-74.
8. Cohen CC, Li KW, Alazraki AL, Beysen C, Carrier CA, Cleeton RL, et al. Dietary sugar restriction reduces hepatic de novo lipogenesis in adolescent boys with fatty liver disease. *J Clin Invest.* 2021;131(24).
9. Radulescu A, Killian M, Kang Q, Yuan Q, and Softic S. Dietary Counseling Aimed at Reducing Sugar Intake Yields the Greatest Improvement in Management of Weight and Metabolic Dysfunction in Children with Obesity. *Nutrients.* 2022;14(7).
10. Inci MK, Park SH, Helsley RN, Attia SL, and Softic S. Fructose Impairs Fat Oxidation: Implications for the Mechanism of Western diet-induced NAFLD. *J Nutr Biochem.* 2022:109224.
11. Softic S, Meyer JG, Wang GX, Gupta MK, Batista TM, Lauritzen H, et al. Dietary Sugars Alter Hepatic Fatty Acid Oxidation via Transcriptional and Post-translational Modifications of Mitochondrial Proteins. *Cell Metab.* 2019;30(4):735-53 e4.
12. Softic S, Stanhope KL, Boucher J, Divanovic S, Lanaspa MA, Johnson RJ, et al. Fructose and hepatic insulin resistance. *Crit Rev Clin Lab Sci.* 2020:1-15.
13. Lanaspa MA, Sanchez-Lozada LG, Cicerchi C, Li N, Roncal-Jimenez CA, Ishimoto T, et al. Uric acid stimulates fructokinase and accelerates fructose metabolism in the development of fatty liver. *PLoS One.* 2012;7(10):e47948.
14. Lee AH, Scapa EF, Cohen DE, and Glimcher LH. Regulation of hepatic lipogenesis by the transcription factor XBP1. *Science.* 2008;320(5882):1492-6.
15. Chiang Morales MD, Chang CY, Le VL, Huang IT, Tsai IL, Shih HJ, et al. High-Fructose/High-Fat Diet Downregulates the Hepatic Mitochondrial Oxidative Phosphorylation Pathway in Mice Compared with High-Fat Diet Alone. *Cells.* 2022;11(21).
16. Ouyang X, Cirillo P, Sautin Y, McCall S, Bruchette JL, Diehl AM, et al. Fructose consumption as a risk factor for non-alcoholic fatty liver disease. *J Hepatol.* 2008;48(6):993-9.
17. Abdelmalek MF, Suzuki A, Guy C, Unalp-Arida A, Colvin R, Johnson RJ, et al. Increased fructose consumption is associated with fibrosis severity in patients with nonalcoholic fatty liver disease. *Hepatology.* 2010;51(6):1961-71.
18. Ishimoto T, Lanaspa MA, Le MT, Garcia GE, Diggle CP, Maclean PS, et al. Opposing effects of fructokinase C and A isoforms on fructose-induced metabolic syndrome in mice. *Proc Natl Acad Sci U S A.* 2012;109(11):4320-5.

19. Ishimoto T, Lanaspa MA, Rivard CJ, Roncal-Jimenez CA, Orlicky DJ, Cicerchi C, et al. High-fat and high-sucrose (western) diet induces steatohepatitis that is dependent on fructokinase. *Hepatology.* 2013;58(5):1632-43.
20. Andres-Hernando A, Orlicky DJ, Kuwabara M, Ishimoto T, Nakagawa T, Johnson RJ, et al. Deletion of Fructokinase in the Liver or in the Intestine Reveals Differential Effects on Sugar-Induced Metabolic Dysfunction. *Cell Metab.* 2020;32(1):117-27 e3.
21. Maryanoff BE, O'Neill JC, McComsey DF, Yabut SC, Luci DK, Gibbs AC, et al. Pyrimidinopyrimidine inhibitors of ketohexokinase: exploring the ring C2 group that interacts with Asp-27B in the ligand binding pocket. *Bioorg Med Chem Lett.* 2012;22(16):5326-9.
22. Maryanoff BE, O'Neill JC, McComsey DF, Yabut SC, Luci DK, Jordan AD, Jr., et al. Inhibitors of Ketohexokinase: Discovery of Pyrimidinopyrimidines with Specific Substitution that Complements the ATP-Binding Site. *ACS Med Chem Lett.* 2011;2(7):538-43.
23. Gutierrez JA, Liu W, Perez S, Xing G, Sonnenberg G, Kou K, et al. Pharmacologic inhibition of ketohexokinase prevents fructose-induced metabolic dysfunction. *Mol Metab.* 2021;48:101196.
24. Shepherd EL, Saborano R, Northall E, Matsuda K, Ogino H, Yashiro H, et al. Ketohexokinase inhibition improves NASH by reducing fructose-induced steatosis and fibrogenesis. *JHEP Rep.* 2021;3(2):100217.
25. Kazierad DJ, Chidsey K, Somayaji VR, Bergman AJ, Birnbaum MJ, and Calle RA. Inhibition of ketohexokinase in adults with NAFLD reduces liver fat and inflammatory markers: A randomized phase 2 trial. *Med (N Y).* 2021;2(7):800-13 e3.
26. Saxena AR, Lyle SA, Khavandi K, Qiu R, Whitlock M, Esler WP, et al. A phase 2a, randomized, double-blind, placebo-controlled, 3-arm, parallel-group study to assess the efficacy, safety, tolerability, and pharmacodynamics of PF-06835919 in patients with nonalcoholic fatty liver disease and type 2 diabetes mellitus. *Diabetes Obes Metab.* 2022.
27. Taylor N. Pfizer dumps midphase NASH prospect, slew of early efforts in Q2 clear-out. https://www.fiercebiotech.com/biotech/pfizer-dumps-midphase-nash-prospect-quarterly-pipeline-cull#:~:text=PF%2D06835919%20moved%20into%20clinical,a%20way%20to%20tackle%20NASH. Accessed 8/14/2022, 2022.
28. Helsley RN, Park SH, Vekaria HJ, Sullivan PG, Conroy LR, Sun RC, et al. Ketohexokinase-C regulates global protein acetylation to decrease carnitine palmitoyltransferase 1a-mediated fatty acid oxidation. *J Hepatol.* 2023;79(1):25-42.
29. Park SH, Helsley RN, Fadhul T, Willoughby JLS, Noetzli L, Tu HC, et al. Fructose induced KHK-C can increase ER stress independent of its effect on lipogenesis to drive liver disease in diet-induced and genetic models of NAFLD. *Metabolism.* 2023:155591.
30. Helsley RN, Moreau F, Gupta MK, Radulescu A, DeBosch B, and Softic S. Tissue-Specific Fructose Metabolism in Obesity and Diabetes. *Curr Diab Rep.* 2020;20(11):64.
31. Ahmad U, and Sharma J. *StatPearls*. Treasure Island (FL) ineligible companies. Disclosure: Jyotsna Sharma declares no relevant financial relationships with ineligible companies.; 2023.
32. Park SH, Helsley RN, Noetzli L, Tu HC, Wallenius K, O'Mahony G, et al. A luminescence-based protocol for assessing fructose metabolism via quantification of ketohexokinase enzymatic activity in mouse or human hepatocytes. *STAR Protoc.* 2021;2(3):100731.
33. Jang C, Hui S, Lu W, Cowan AJ, Morscher RJ, Lee G, et al. The Small Intestine Converts Dietary Fructose into Glucose and Organic Acids. *Cell Metab.* 2018;27(2):351-61 e3.
34. Kawasaki T, Akanuma H, and Yamanouchi T. Increased fructose concentrations in blood and urine in patients with diabetes. *Diabetes Care.* 2002;25(2):353-7.
35. Hinds TD, Jr., Burns KA, Hosick PA, McBeth L, Nestor-Kalinoski A, Drummond HA, et al. Biliverdin Reductase A Attenuates Hepatic Steatosis by Inhibition of Glycogen Synthase Kinase

(GSK) 3beta Phosphorylation of Serine 73 of Peroxisome Proliferator-activated Receptor (PPAR) alpha. *J Biol Chem.* 2016;291(48):25179-91.
36. Rayasam GV, Tulasi VK, Sodhi R, Davis JA, and Ray A. Glycogen synthase kinase 3: more than a namesake. *Br J Pharmacol.* 2009;156(6):885-98.
37. Liu L, Li T, Liao Y, Wang Y, Gao Y, Hu H, et al. Triose Kinase Controls the Lipogenic Potential of Fructose and Dietary Tolerance. *Cell Metab.* 2020;32(4):605-18 e7.
38. Singh SK, and Sarma MS. Hereditary fructose intolerance: A comprehensive review. *World J Clin Pediatr.* 2022;11(4):321-9.
39. Gibney PA, Schieler A, Chen JC, Bacha-Hummel JM, Botstein M, Volpe M, et al. Common and divergent features of galactose-1-phosphate and fructose-1-phosphate toxicity in yeast. *Mol Biol Cell.* 2018;29(8):897-910.
40. Phillips MJ, Little JA, and Ptak TW. Subcellular pathology of hereditary fructose intolerance. *Am J Med.* 1968;44(6):910-21.
41. Veiga-da-Cunha M, and Van Schaftingen E. Identification of fructose 6-phosphate- and fructose 1-phosphate-binding residues in the regulatory protein of glucokinase. *J Biol Chem.* 2002;277(10):8466-73.
42. Vandercammen A, Detheux M, and Van Schaftingen E. Binding of sorbitol 6-phosphate and of fructose 1-phosphate to the regulatory protein of liver glucokinase. *Biochem J.* 1992;286 (Pt 1)(Pt 1):253-6.
43. Gergely P, Toth B, Farkas I, and Bot G. Effect of fructose 1-phosphate on the activation of liver glycogen synthase. *Biochem J.* 1985;232(1):133-7.
44. Davies DR, Detheux M, and Van Schaftingen E. Fructose 1-phosphate and the regulation of glucokinase activity in isolated hepatocytes. *Eur J Biochem.* 1990;192(2):283-9.
45. Lanaspa MA, Andres-Hernando A, Orlicky DJ, Cicerchi C, Jang C, Li N, et al. Ketohexokinase C blockade ameliorates fructose-induced metabolic dysfunction in fructose-sensitive mice. *J Clin Invest.* 2018;128(6):2226-38.
46. Bricambert J, Miranda J, Benhamed F, Girard J, Postic C, and Dentin R. Salt-inducible kinase 2 links transcriptional coactivator p300 phosphorylation to the prevention of ChREBP-dependent hepatic steatosis in mice. *J Clin Invest.* 2010;120(12):4316-31.
47. Fan S, Gao Y, Qu A, Jiang Y, Li H, Xie G, et al. YAP-TEAD mediates PPAR alpha-induced hepatomegaly and liver regeneration in mice. *Hepatology.* 2022;75(1):74-88.
48. Berthou L, Duverger N, Emmanuel F, Langouet S, Auwerx J, Guillouzo A, et al. Opposite regulation of human versus mouse apolipoprotein A-I by fibrates in human apolipoprotein A-I transgenic mice. *J Clin Invest.* 1996;97(11):2408-16.
49. Zhang J, Zheng Y, Martens L, and Pfeiffer AFH. The Regulation and Secretion of Glucagon in Response to Nutrient Composition: Unraveling Their Intricate Mechanisms. *Nutrients.* 2023;15(18).
50. Futatsugi K, Smith AC, Tu M, Raymer B, Ahn K, Coffey SB, et al. Discovery of PF-06835919: A Potent Inhibitor of Ketohexokinase (KHK) for the Treatment of Metabolic Disorders Driven by the Overconsumption of Fructose. *J Med Chem.* 2020;63(22):13546-60.
51. Softic S, Kirby M, Berger NG, Shroyer NF, Woods SC, and Kohli R. Insulin concentration modulates hepatic lipid accumulation in mice in part via transcriptional regulation of fatty acid transport proteins. *PLoS One.* 2012;7(6):e38952.
52. Softic S, Boucher J, Solheim MH, Fujisaka S, Haering MF, Homan EP, et al. Lipodystrophy Due to Adipose Tissue-Specific Insulin Receptor Knockout Results in Progressive NAFLD. *Diabetes.* 2016;65(8):2187-200.

53. Young LEA, Conroy LR, Clarke HA, Hawkinson TR, Bolton KE, Sanders WC, et al. In situ mass spectrometry imaging reveals heterogeneous glycogen stores in human normal and cancerous tissues. *EMBO Mol Med.* 2022;14(11):e16029.
54. Moreau F, Brunao BB, Liu XY, Tremblay F, Fitzgerald K, Avila-Pacheco J, et al. Liver-specific FGFR4 knockdown in mice on a HFD increases bile acid synthesis and improves hepatic steatosis. *J Lipid Res.* 2022:100324.

FIGURE TITLES AND LEGENDS

Figure 1. **Inhibition of ketohexokinase activity, but not its knockdown, leads to hepatic glycogen accumulation.**

(A) Weight gain of mice on low-fat diet (LFD), high-fat diet (HFD), HFD treated with siRNA, and HFD treated with inhibitor for the last four weeks of this ten-week experiment. (B) Lean mass and fat mass normalized by body weight as assessed by EchoMRI. Perigonadal adipose tissue (C) and liver (D) weights at the time of sacrifice. n=7-8 mice per group. (E) Representative periodic acid-schiff (PAS) stained images of liver histology. Bar=50µm. (F) Mass spectrometry (MS) analysis for glycogen in the liver. (G) Glycogen chain length as determined by MS. (H) Heatmap of all glycans and (I) principal component analysis of all glycans in LFD, HFD, HFD+siRNA, and HFD+Inhib groups. n=4 mice per group. mRNA expression of Gck (J) and the genes involved in (K) glycogen synthesis and degradation. n=6 mice per group. Statistical analysis was performed using one-way ANOVA compared to LFD group (#$p < 0.05$; ## $p < 0.01$; ### $p < 0.001$; #### $p < 0.0001$) with post hoc t-tests between the individual groups (*$p < 0.05$; **$p < 0.01$; ***$p < 0.001$; ****$p < 0.0001$).

Figure 2. Small molecule inhibitor decreases ketohexokinase enzymatic activity in liver and kidney, but not in intestine.

(A) Serum fructose level from the mice at sacrifice. The levels of (B) fructose (C), fructose 1-phosphate (F1P) and the ratio of (D) F1P/fructose in the liver. n=7-8 mice per group. Quantification of KHK activity in (E) liver, (F) kidney, and (G) intestine. (H) Absolute KHK activity in liver, intestine, kidney and perigonadal adipose tissue. (I) Western blot of total KHK and KHK-C in liver, intestine, kidney and perigonadal adipose tissue. n=4 mice per group. Actin was used as a loading control. (J) Urinary fructose level corrected by urine creatinine and (K) fructose excretion in urine over 24h. (L) *In vivo* monitoring of the inhibitor concentration over 24h period following single gavage with 10 mg/kg or 30 mg/ml of the inhibitor. n=2 mice per group. (M) Unbound plasma concentration of the inhibitor (red dots) quantified by mass spectrometry in LFD fed mice, 2-5h after last dose of the inhibitor. Pharmacokinetic model fitting (blue line) based on inhibitor concentration (red dots). Dashed line represents target

concentration. Statistical analysis was performed using one-way ANOVA compared to the LFD group (#p < 0.05; ### p < 0.001; #### p < 0.0001) with post hoc t-tests between the individual groups (*p < 0.05; **p < 0.01; ***p < 0.001; ****p < 0.0001).

Figure 3. KHK siRNA completely deletes KHK-C and increases HK2, while the inhibitor partially decreases both KHK-C and TKFC proteins.

(A) The fructose metabolism pathway. (B) mRNA of fructose metabolizing enzymes from livers of the mice. n=6 mice per group. (C) Western blot and (D) densitometry quantification of fructose metabolizing enzymes in liver lysates. n=4 mice per group. (E) densitometry quantification and (F) western blot of hexokinases. n=4 mice per group. (G) mRNA expression of hexokinases in the liver from mice fed a LFD. (H) hepatic mRNA expression of aldo-keto reductase (Akr1b1) and sorbitol dehydrogenase (Sord). Statistical analysis was performed using one-way ANOVA compared to the LFD group (#p < 0.05; ## p < 0.01; ### p < 0.001; #### p < 0.0001) with post hoc t-tests between the individual groups (***p < 0.001).

Figure 4. Knockdown of ketohexokinase, but not inhibition of its activity, improves glucose tolerance and increases the glycolysis pathway.

(A) Glucose tolerance test (GTT) measured after 8 weeks on the diets and two weeks after initiation of the treatments. (B) Area under the curve calculated from GTT. n=7-8 mice per group. Fasted serum glucose (C), insulin (D), and calculated HOMA-IR (E) at 10 weeks on the diet. (F) Western blot analysis of insulin signaling in the liver. n=4 mice per group. Western blot analysis (G) and qPCR quantification (H) of genes mediating the gluconeogenesis pathway. n=6 mice per group for gene expression. Actin was used as a loading control. (I) short-chain and (J) long-chain acylcarnitines quantified by mass spectrometry. n=7-8 mice per group. Statistical analysis was performed using one-way ANOVA compared to the LFD group (### p < 0.001; #### p < 0.0001) with post hoc t-tests between the individual groups (*p < 0.05; **p < 0.01; ***p < 0.001; ****p < 0.0001).

Figure 5. RNAseq analysis revealed profound and unique effects of ketohexokinase knockdown versus inhibition on hepatic transcriptome

(A) Principal component analysis of RNAseq data from the livers of our experimental mice (B) A heatmap representation of the top 40 genes plus KHK. (C) Heatmap of the de novo lipogenesis pathway and (D) the fatty acid oxidation pathway. Volcano plot comparison of (E) HFD to LFD, (F) HFD to HFD+siRNA, (G) HFD to HFD+Inhibitor, and (H) HFD+siRNA to HFD+Inhibitor. Reactome pathway analysis showing the most significantly altered pathways between (I) HFD+siRNA versus HFD group and (J) HFD+Inhibitor versus HFD group.

Figure 6. Ketohexokinase knockdown lowers the DNL, while the inhibitor increases the FAO pathway.

(A) ChREBP-β (MLXIPL-β) and (B) SREBF1c mRNA expression in the liver of our experimental mice. (C) Western blot showing nuclear translocation of ChREBP and SREBP1 proteins in the liver. (D) mRNA and (E) Western blot quantification of proteins involved in de novo lipogenesis. (F) Protein and (G) mRNA expression of genes regulating mitochondrial fatty acid oxidation. (H) Protein and (I) mRNA expression of genes regulating peroxisomal fatty acid oxidation. n=7-8 mice per group for mRNA expression and n=4 mice per group for protein quantification. Statistical analysis was performed using one-way ANOVA compared to the LFD group (## $p < 0.01$; ### $p < 0.001$; #### $p < 0.0001$) with post hoc t-tests between the individual groups (*$p < 0.05$; **$p < 0.01$; ****$p < 0.0001$).

Figure 7. Overexpression of wild-type KHK supports glycogen accumulation, while overexpression of kinase-dead mutant KHK increases the expression of the DNL pathway.

(A) KHK-C mRNA overexpression in control HepG2 cells, GFP-tagged wild-type mouse KHK-C overexpressed cells (WT KHK-C), or mouse kinase-dead mutant overexpressed (KM KHK-C) cells using lentivirus transfection. (B) Protein levels of fructose metabolizing enzymes in control HepG2 cells, WT KHK-C cells, KM KHK-C cells, and mouse liver. (C) KHK activity in control HepG2 cells, WT KHK-C cells and KM KHK-C cells treated with 5 mM fructose. (D) ALT level and (E) total protein after treatment

with 5mM fructose or 5mM 3-O methylfructose (3-OMF) for 24 hr. (F) Periodic acid-Schiff (PAS) staining of HepG2 cells treated with fructose for 24 hr. (G) glycogen levels in control HepG2 cells, WT KHK-C cells and KM KHK-C cells treated with fructose or 3-OMF. mRNA of Gckrp (H), Hk1 (I), and HK2 (J) expression in these cells treated with fructose or 3-OMF. (K) Western blot quantification of enzymes involved in sugar metabolism in control HepG2 cells, WT KHK-C cells, KM KHK-C cells, and mouse liver. (L) mRNA expression of de novo lipogenesis genes and (M) fatty acid oxidation genes. n=4 for mice per group for gene expression and protein quantification. Statistical analysis was performed using one-way ANOVA compared to the LFD group (#$p < 0.05$; ## $p < 0.01$; ### $p < 0.001$; #### $p < 0.0001$) with post hoc t-tests between the individual groups (****$p < 0.0001$).

Figure 1

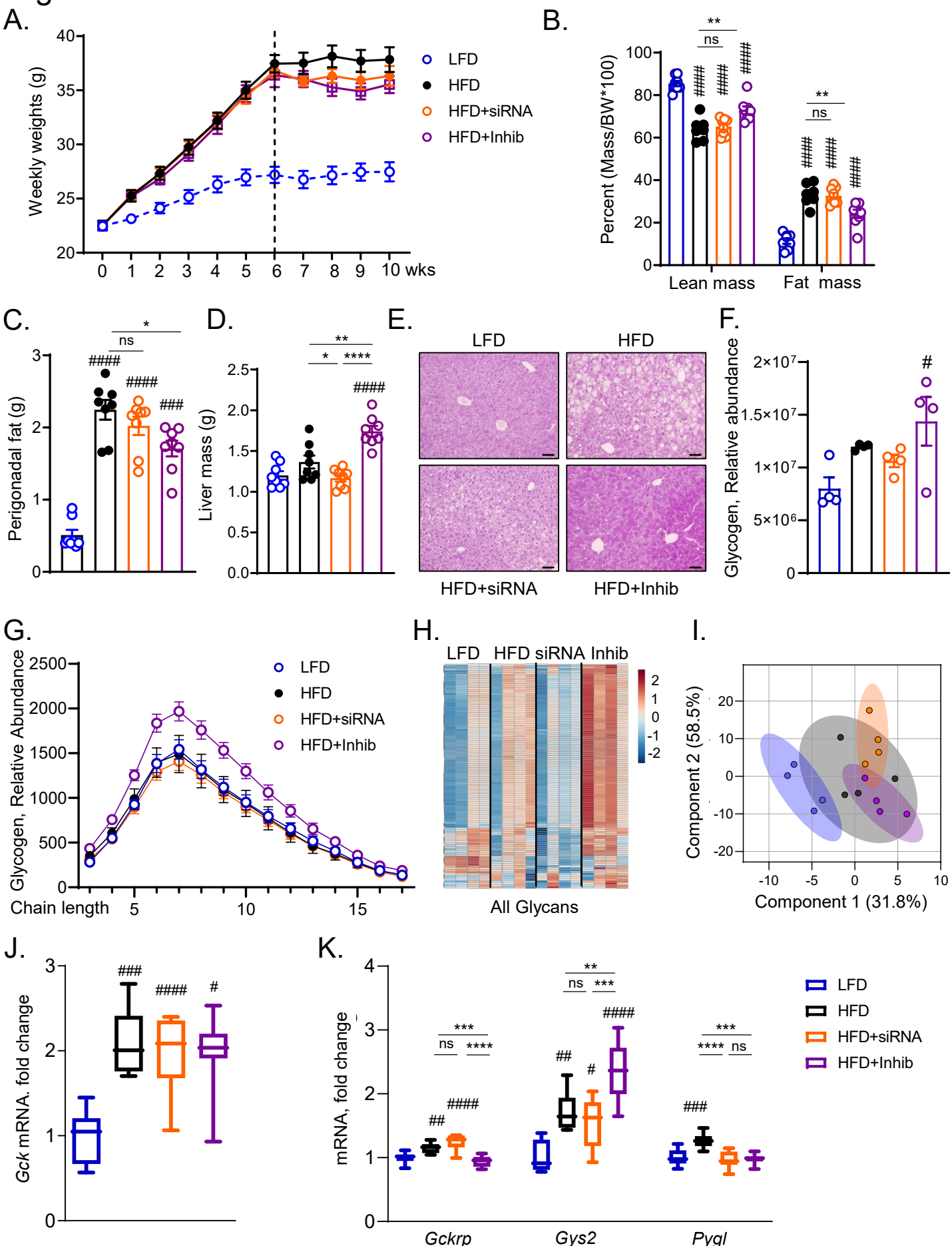
A.
Weekly weights (g)
40
35
30
25
20
0 1 2 3 4 5 6 7 8 9 10 wks
LFD
HFD
HFD+siRNA
HFD+Inhib
B.
Percent (Mass/BW*100)
100
80
60
40
20
0
**
ns
**
ns
Lean mass
Fat mass
C.
Perigonadal fat (g)
3
2
1
0
*
ns
####
####
###
D.
Liver mass (g)
2.5
2.0
1.5
1.0
0.5
0.0
**
*
****
####
E.
LFD
HFD
HFD+siRNA
HFD+Inhib
F.
Glycogen, Relative abundance
2×10^7
1.5×10^7
1×10^7
5×10^6
0
#
G.
Glycogen, Relative Abundance
2500
2000
1500
1000
500
0
Chain length 5 10 15
LFD
HFD
HFD+siRNA
HFD+Inhib
H.
LFD HFD siRNA Inhib
2
1
0
-1
-2
All Glycans
I.
Component 2 (58.5%)
20
10
0
-10
-20
-10 -5 0 5 10
Component 1 (31.8%)
J.
Gck mRNA. fold change
3
2
1
0
###
####
#
K.
mRNA, fold change
4
3
2
1
0
**
ns
***
***
ns
****
****
ns
***
###
##
#
####
##
###
Gckrp
Gys2
Pygl
LFD
HFD
HFD+siRNA
HFD+Inhib

Figure 2

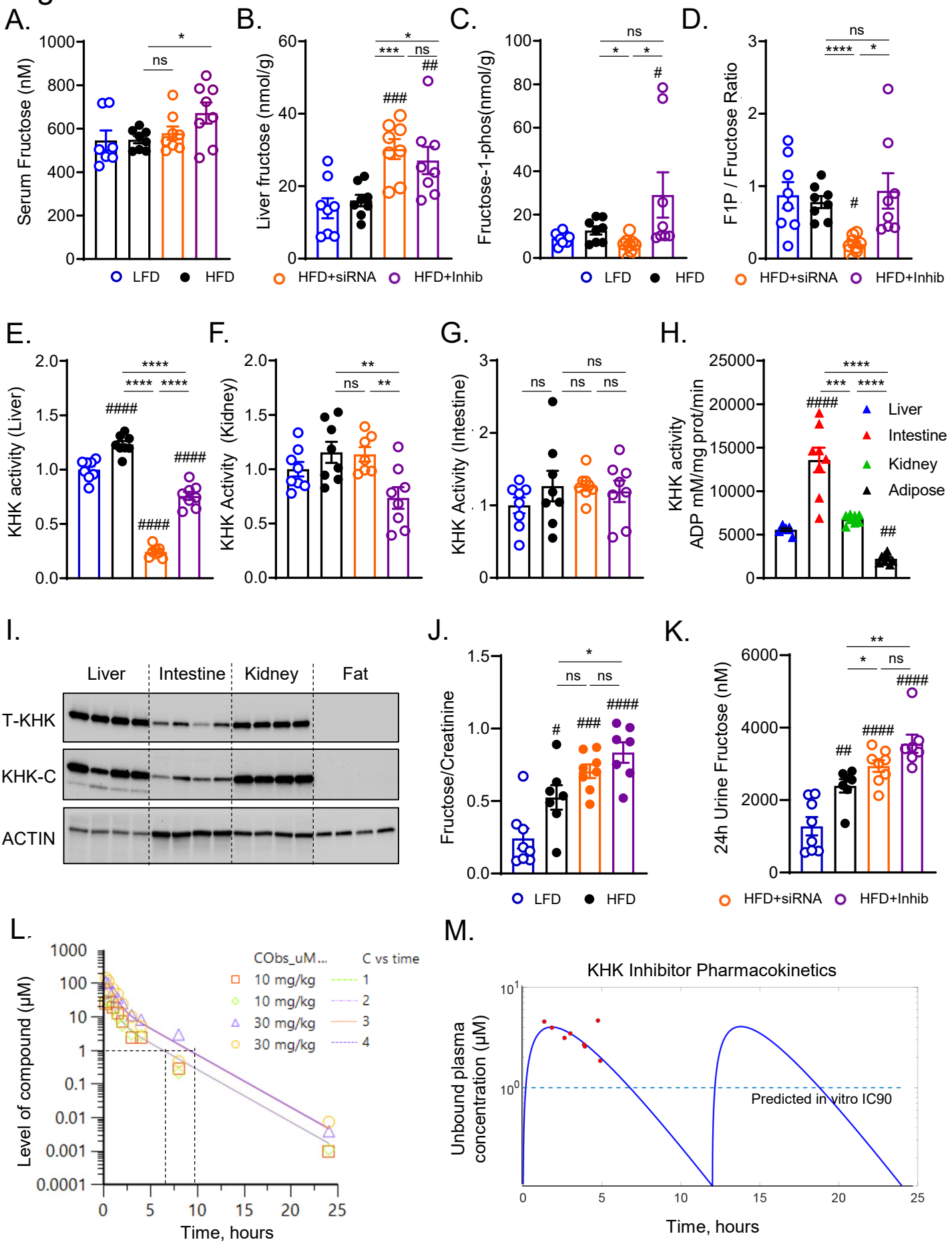
A.
Serum Fructose (nM)
LFD
HFD
B.
Liver fructose (nmol/g)
HFD+siRNA
HFD+Inhib
C.
Fructose-1-phos(nmol/g)
D.
F1P / Fructose Ratio
E.
KHK activity (Liver)
F.
KHK Activity (Kidney)
G.
KHK Activity (Intestine)
H.
KHK activity
ADP mM/mg prot/min
Liver
Intestine
Kidney
Adipose
I.
Liver
Intestine
Kidney
Fat
T-KHK
KHK-C
ACTIN
J.
Fructose/Creatinine
K.
24h Urine Fructose (nM)
L.
Level of compound (μM)
CObs_uM...
C vs time
10 mg/kg
30 mg/kg
Time, hours
M.
KHK Inhibitor Pharmacokinetics
Unbound plasma concentration (μM)
Predicted in vitro IC90
Time, hours

Figure 3

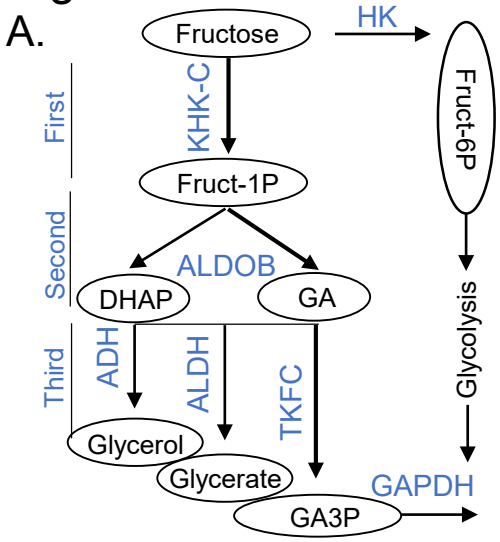
A.
Fructose
HK
Fruct-6P
KHK-C
First
Fruct-1P
Second
ALDOB
DHAP
GA
Third
ADH
ALDH
TKFC
Glycolysis
Glycerol
Glycerate
GAPDH
GA3P

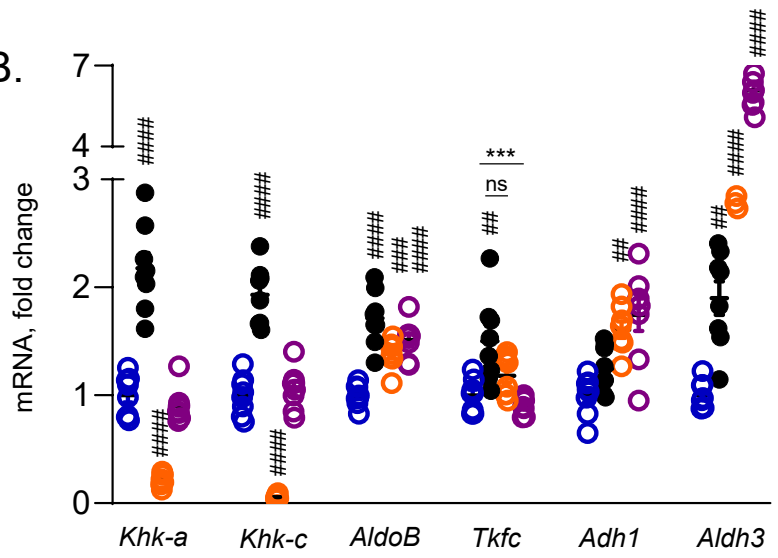
B.
mRNA, fold change
Khk-a
Khk-c
AldoB
Tkfc
Adh1
Aldh3
***
ns

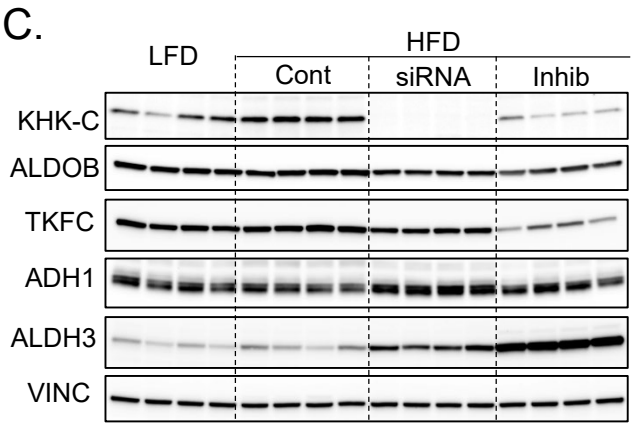
C.
LFD
HFD
Cont
siRNA
Inhib
KHK-C
ALDOB
TKFC
ADH1
ALDH3
VINC

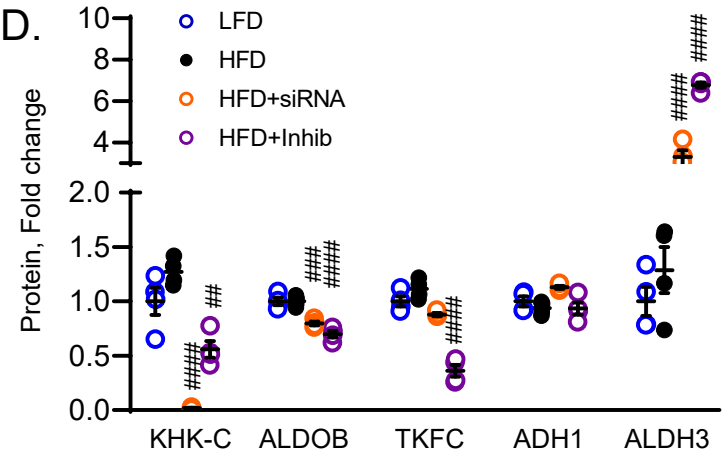
D.
LFD
HFD
HFD+siRNA
HFD+Inhib
Protein, Fold change
KHK-C
ALDOB
TKFC
ADH1
ALDH3

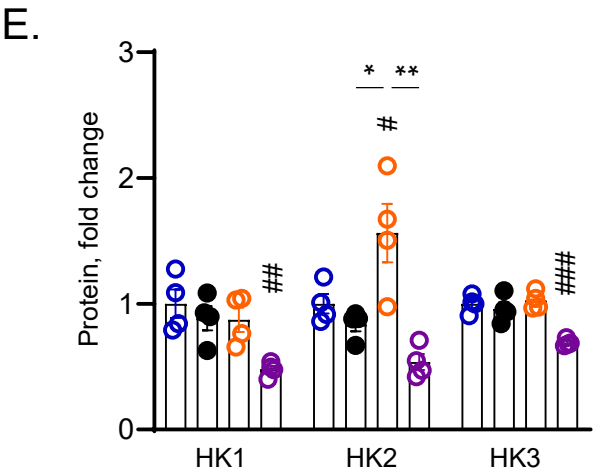
E.
Protein, fold change
HK1
HK2
HK3

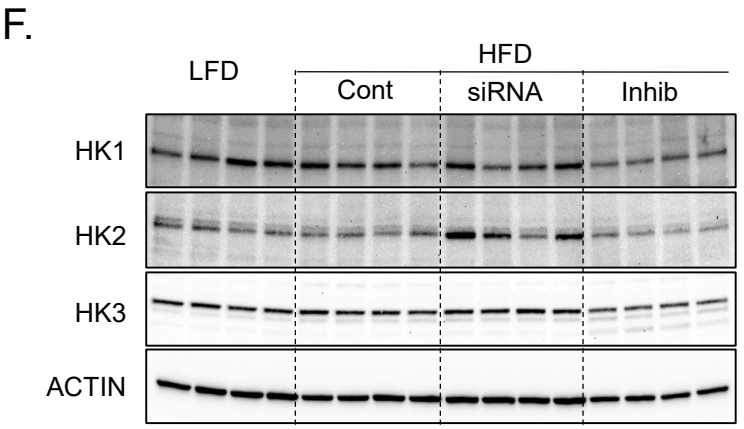
F.
LFD
HFD
Cont
siRNA
Inhib
HK1
HK2
HK3
ACTIN

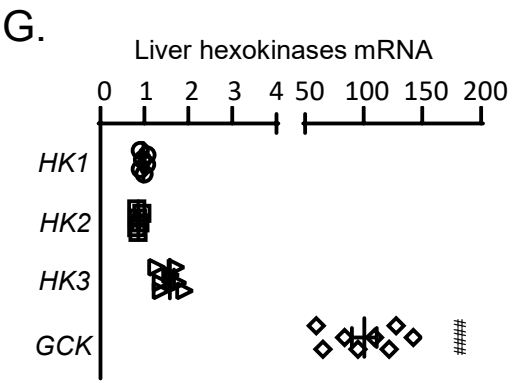
G.
Liver hexokinases mRNA
HK1
HK2
HK3
GCK

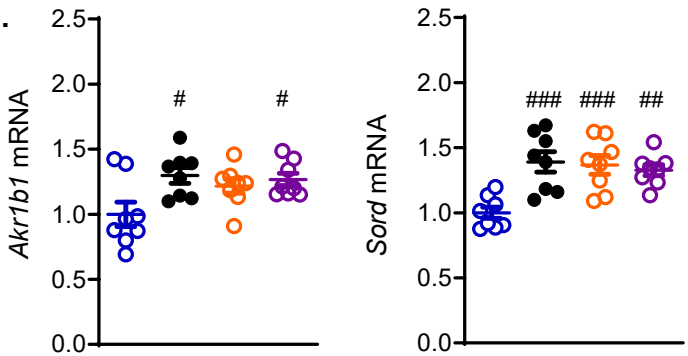
H.
Akr1b1 mRNA
Sord mRNA

Figure 4

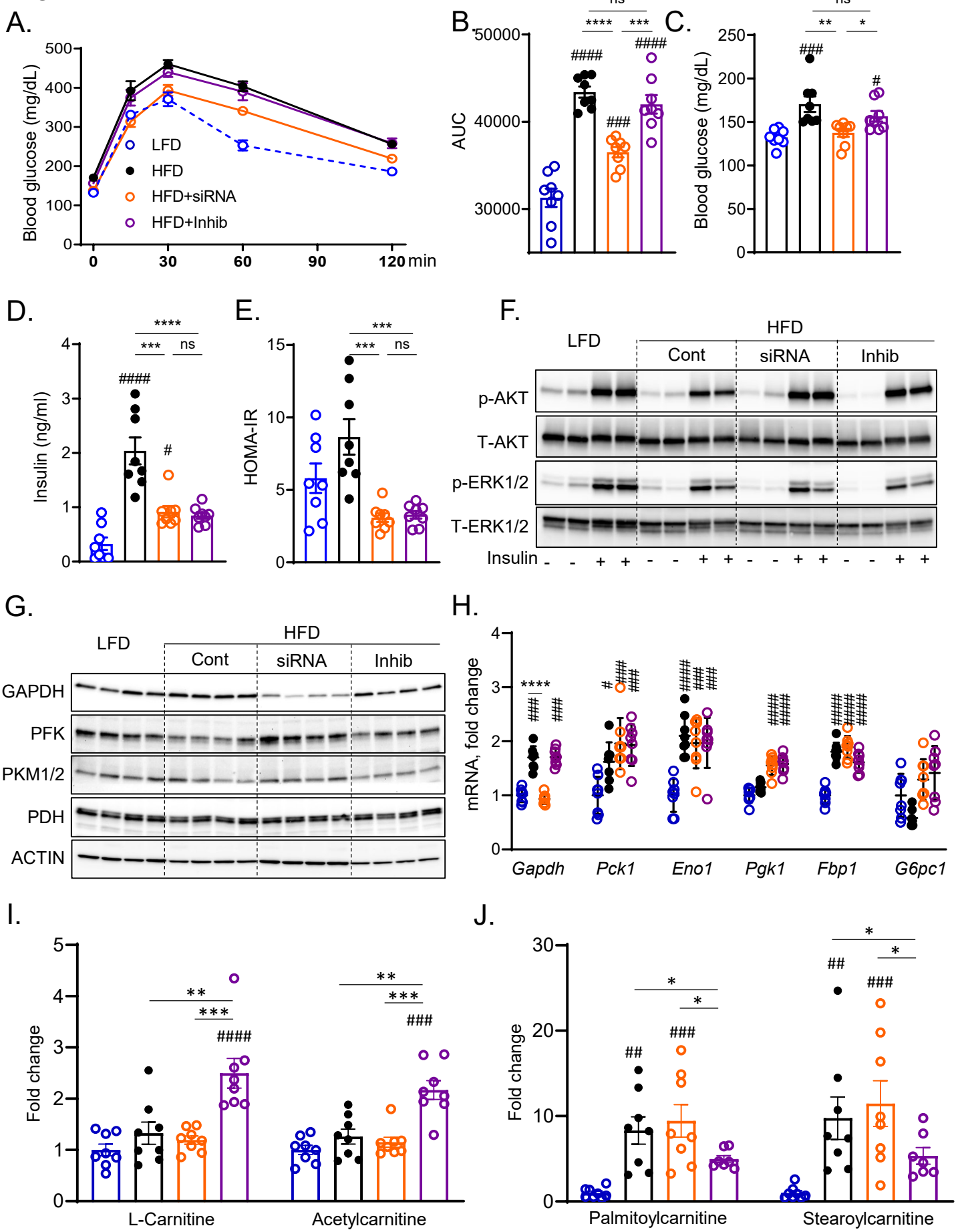
A.
Blood glucose (mg/dL)
LFD
HFD
HFD+siRNA
HFD+Inhib
min
B.
AUC
C.
Blood glucose (mg/dL)
D.
Insulin (ng/ml)
E.
HOMA-IR
F.
LFD
HFD
Cont
siRNA
Inhib
p-AKT
T-AKT
p-ERK1/2
T-ERK1/2
Insulin
G.
GAPDH
PFK
PKM1/2
PDH
ACTIN
H.
mRNA, fold change
Gapdh
Pck1
Eno1
Pgk1
Fbp1
G6pc1
I.
Fold change
L-Carnitine
Acetylcarnitine
J.
Fold change
Palmitoylcarnitine
Stearoylcarnitine

Figure 5

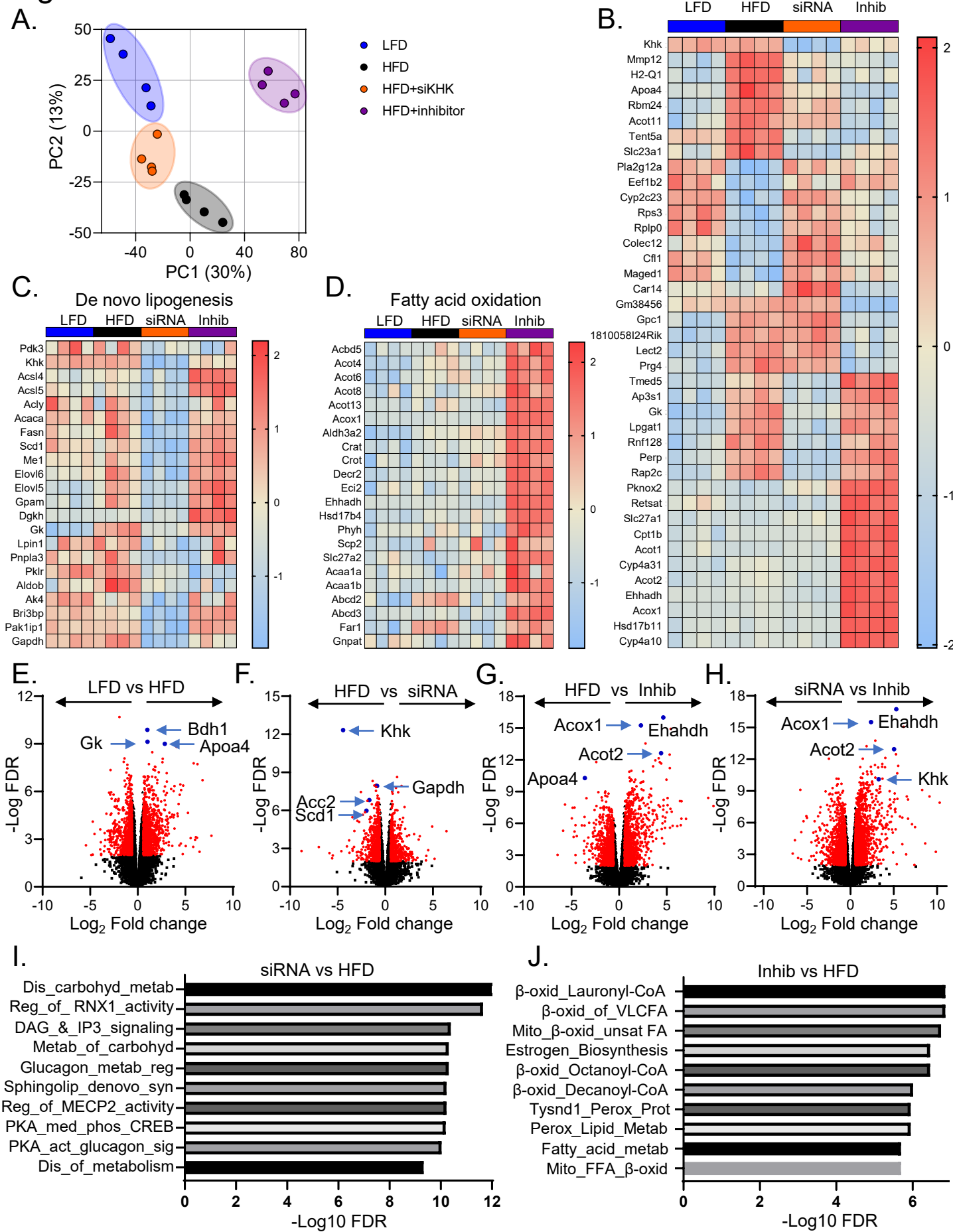
A.
PC2 (13%)
PC1 (30%)
LFD
HFD
HFD+siKHK
HFD+inhibitor
B.
Top 40 genes
LFD HFD siRNA Inhib
Khk
Mmp12
H2-Q1
Apoa4
Rbm24
Acot11
Tent5a
Slc23a1
Pla2g12a
Eef1b2
Cyp2c23
Rps3
Rplp0
Colec12
Cfl1
Maged1
Car14
Gm38456
Gpc1
1810058I24Rik
Lect2
Prg4
Tmed5
Ap3s1
Gk
Lpgat1
Rnf128
Perp
Rap2c
Pknox2
Retsat
Slc27a1
Cpt1b
Acot1
Cyp4a31
Acot2
Ehhadh
Acox1
Hsd17b11
Cyp4a10
C.
De novo lipogenesis
LFD HFD siRNA Inhib
Pdk3
Khk
Acsl4
Acsl5
Acly
Acaca
Fasn
Scd1
Me1
Elovl6
Elovl5
Gpam
Dgkh
Gk
Lpin1
Pnpla3
Pklr
Aldob
Ak4
Bri3bp
Pak1ip1
Gapdh
D.
Fatty acid oxidation
LFD HFD siRNA Inhib
Acbd5
Acot4
Acot6
Acot8
Acot13
Acox1
Aldh3a2
Crat
Crot
Decr2
Eci2
Ehhadh
Hsd17b4
Phyh
Scp2
Slc27a2
Acaa1a
Acaa1b
Abcd2
Abcd3
Far1
Gnpat
E.
LFD vs HFD
Bdh1
Gk
Apoa4
-Log FDR
Log2 Fold change
F.
HFD vs siRNA
Khk
Gapdh
Acc2
Scd1
-Log FDR
Log2 Fold change
G.
HFD vs Inhib
Acox1
Ehahdh
Acot2
Apoa4
-Log FDR
Log2 Fold change
H.
siRNA vs Inhib
Acox1
Ehahdh
Acot2
Khk
-Log FDR
Log2 Fold change
I.
siRNA vs HFD
Dis_carbohyd_metab
Reg_of_ RNX1_activity
DAG_&_IP3_signaling
Metab_of_carbohyd
Glucagon_metab_reg
Sphingolip_denovo_syn
Reg_of_MECP2_activity
PKA_med_phos_CREB
PKA_act_glucagon_sig
Dis_of_metabolism
-Log10 FDR
J.
Inhib vs HFD
β-oxid_Lauronyl-CoA
β-oxid_of_VLCFA
Mito_β-oxid_unsat FA
Estrogen_Biosynthesis
β-oxid_Octanoyl-CoA
β-oxid_Decanoyl-CoA
Tysnd1_Perox_Prot
Perox_Lipid_Metab
Fatty_acid_metab
Mito_FFA_β-oxid
-Log10 FDR

Figure 6

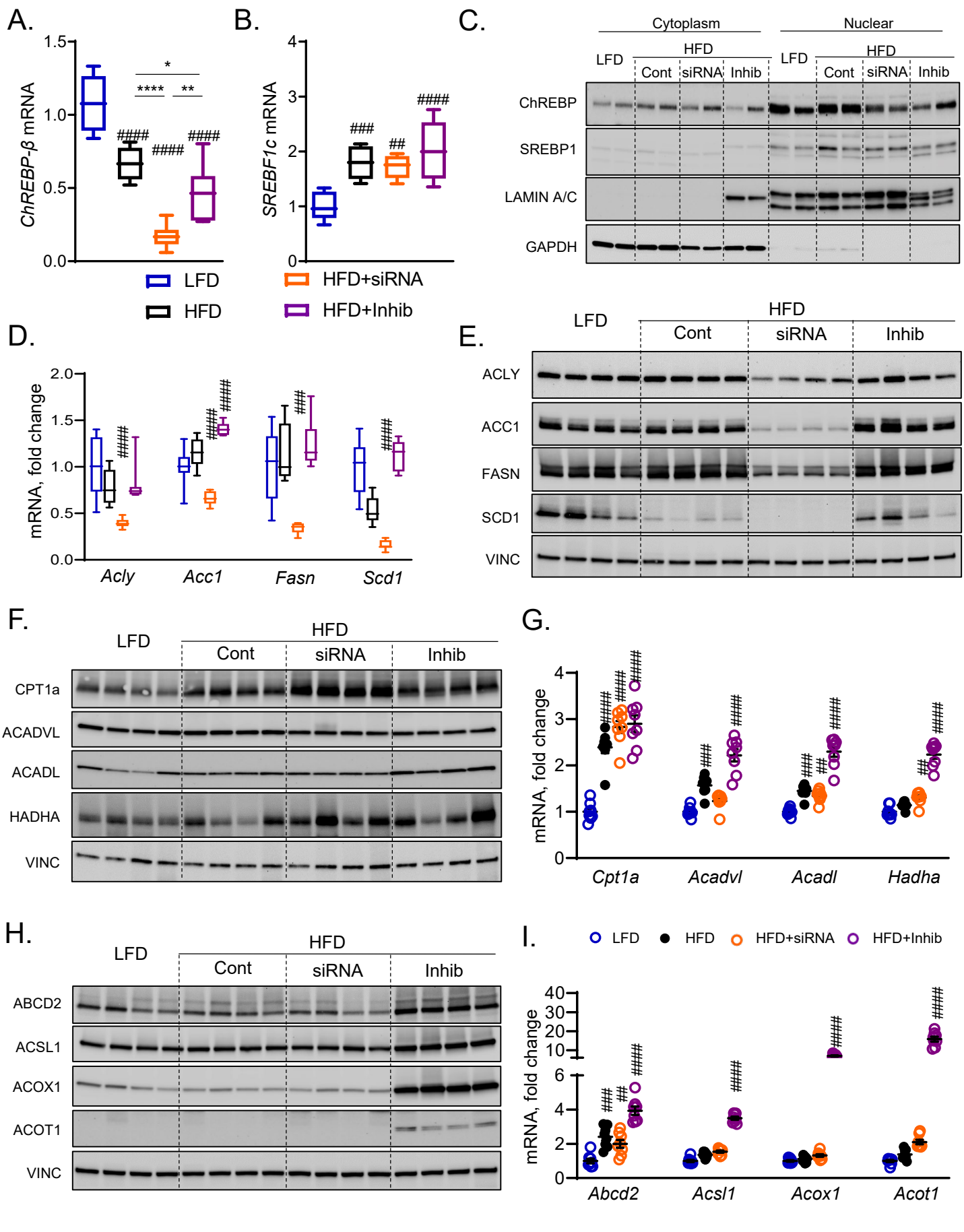
A.
B.
C.
ChREBP-β mRNA
SREBF1c mRNA
LFD
HFD
HFD+siRNA
HFD+Inhib
Cytoplasm
Nuclear
Cont
siRNA
Inhib
ChREBP
SREBP1
LAMIN A/C
GAPDH
D.
E.
mRNA, fold change
Acly
Acc1
Fasn
Scd1
ACLY
ACC1
FASN
SCD1
VINC
F.
G.
CPT1a
ACADVL
ACADL
HADHA
Cpt1a
Acadvl
Acadl
Hadha
H.
I.
ABCD2
ACSL1
ACOX1
ACOT1
Abcd2
Acsl1
Acox1
Acot1

Figure 7

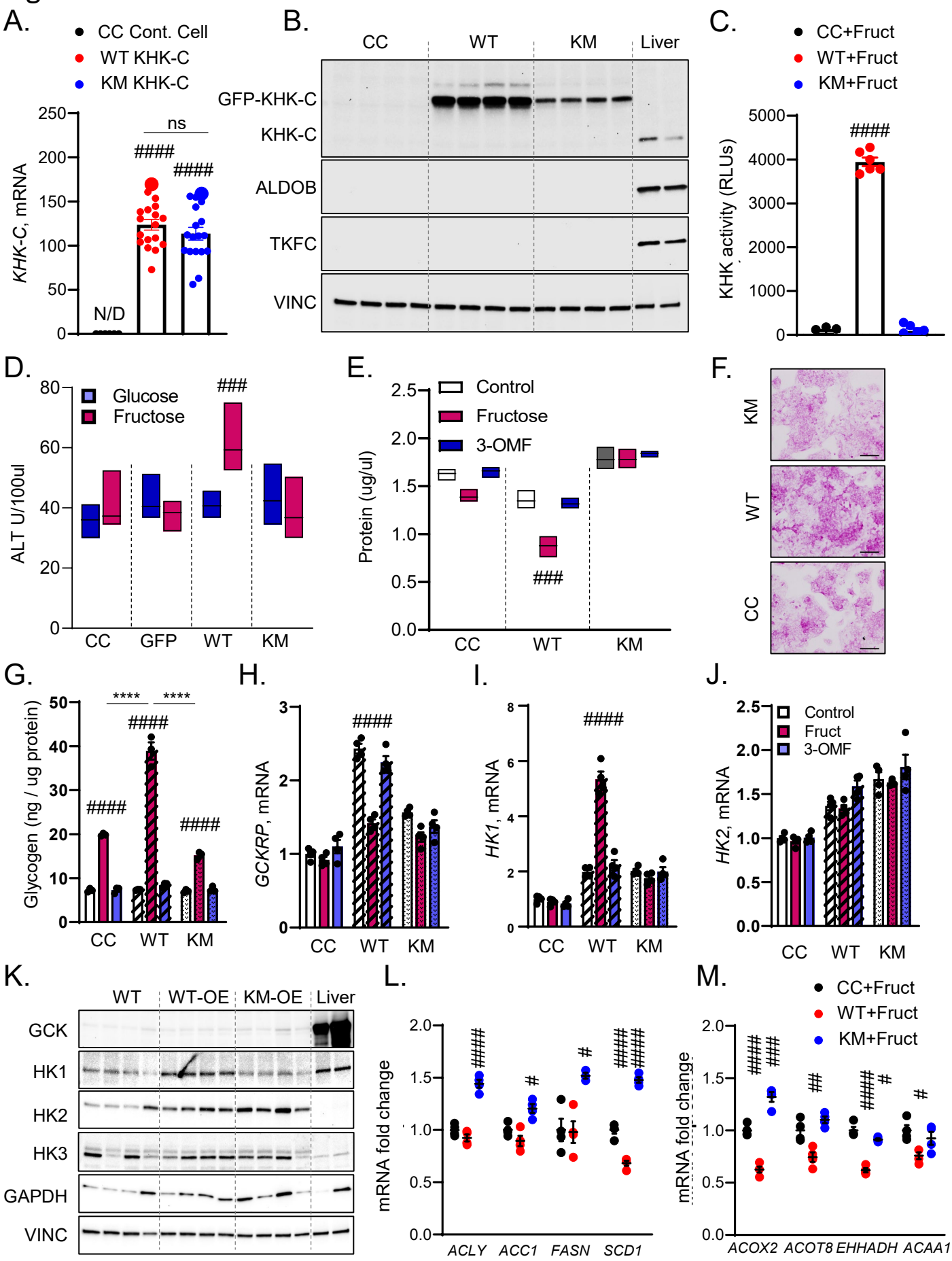
A.
CC Cont. Cell
WT KHK-C
KM KHK-C
KHK-C, mRNA
N/D
ns
####
####
B.
CC
WT
KM
Liver
GFP-KHK-C
KHK-C
ALDOB
TKFC
VINC
C.
CC+Fruct
WT+Fruct
KM+Fruct
KHK activity (RLUs)
####
D.
Glucose
Fructose
ALT U/100ul
###
CC
GFP
WT
KM
E.
Control
Fructose
3-OMF
Protein (ug/ul)
###
CC
WT
KM
F.
KM
WT
CC
G.
Glycogen (ng / ug protein)
****
****
####
####
####
CC
WT
KM
H.
GCKRP, mRNA
####
CC
WT
KM
I.
HK1, mRNA
####
CC
WT
KM
J.
Control
Fruct
3-OMF
HK2, mRNA
CC
WT
KM
K.
WT
WT-OE
KM-OE
Liver
GCK
HK1
HK2
HK3
GAPDH
VINC
L.
mRNA fold change
ACLY
ACC1
FASN
SCD1
M.
CC+Fruct
WT+Fruct
KM+Fruct
mRNA fold change
ACOX2
ACOT8
EHHADH
ACAA1